Agricultural and Forest Meteorology 223 (2016) 116–131

Contents lists available at ScienceDirect

Agricultural and Forest Meteorology

journal homepage: www.elsevier.com/locate/agrformet

Development of a coupled carbon and water model for estimating global gross primary productivity and evapotranspiration based on eddy flux and remote sensing data

Yulong Zhang[a,b,*], Conghe Song[a,c,*], Ge Sun[d], Lawrence E. Band[a,b], Steven McNulty[d], Asko Noormets[d], Quanfa Zhang[e], Zhiqiang Zhang[f]

[a] Department of Geography, University of North Carolina at Chapel Hill, Chapel Hill 27599, NC, USA
[b] Institute for the Environment, University of North Carolina at Chapel Hill, Chapel Hill 27599, NC, USA
[c] School of Ecological and Environmental Sciences, East China Normal University, Shanghai 200241, China
[d] Eastern Forest Environmental Threat Assessment Center, Southern Research Station, USDA Forest Service, Raleigh 27606, NC, USA
[e] Key Laboratory of Aquatic Botany and Watershed Ecology, Wuhan Botanical Garden, Chinese Academy of Sciences, Wuhan 430074, China
[f] School of Soil and Water Conservation, Beijing Forestry University, Beijing 100083, China

ARTICLE INFO

Article history:
Received 8 July 2015
Received in revised form 17 February 2016
Accepted 5 April 2016

Keywords:
Gross primary productivity
Evapotranspiration
Light-use efficiency
Water-use efficiency
FLUXNET
MODIS
CCW

ABSTRACT

Terrestrial gross primary productivity (GPP) and evapotranspiration (ET) are two key ecosystem fluxes in the global carbon and water cycles. As carbon and water fluxes are inherently linked, knowing one provides information for the other. However, tightly coupled and easy to use ecosystem models are rare and there are still large uncertainties in global carbon and water flux estimates. In this study, we developed a new monthly coupled carbon and water (CCW) model. GPP was estimated based on the light-use efficiency (LUE) theory that considered the effect of diffuse radiation, while ET was modeled based on GPP and water-use efficiency (WUE). We evaluated the non-linear effect of single (GPP_{OR}) or combined (GPP_{AND}) limitations of temperature and vapor pressure deficit on GPP. We further compared the effects of three types of WUE (i.e., WUE, inherent WUE, and underlying WUE) on ET (i.e., ET_{WUE}, ET_{IWUE} and ET_{UWUE}). CCW was calibrated and validated using global eddy covariance measurement from FLUXNET and remote sensing data from Moderate Resolution Imaging Spectroradiometer (MODIS) from 2000 to 2007. Modeled GPP_{AND} and GPP_{OR} explained 67.3% and 66.8% of variations of tower-derived GPP, respectively, while ET_{UWUE}, ET_{IWUE} and ET_{WUE} explained 65.7%, 59.9% and 58.1% of tower-measured ET, respectively. Consequently, we chose GPP_{AND} and ET_{UWUE} as the best modeling framework for CCW, and estimated global GPP as 134.2 Pg C yr^{-1} and ET as 57.0×10^3 km^3 for vegetated areas in 2001. Global ET estimated by CCW compared favorably with MODIS ET (60.5×10^3 km^3) and ET derived from global precipitation (56.5×10^3 km^3). However, global GPP estimated by CCW was about 19% higher than MODIS GPP (109.0 Pg C yr^{-1}). The mean global WUE value estimated by CCW (2.35 g C kg^{-1} H_2O) was close to the mean tower-based WUE (2.60 g C kg^{-1} H_2O), but was much higher than the WUE derived from MODIS products (1.80 g C kg^{-1} H_2O). We concluded that the new simple CCW model provided improved estimates of GPP and ET. The biome-specific parameters derived in this study allow CCW to be further linked with land use change models to project human impacts on terrestrial ecosystem functions.

1. Introduction

Carbon and water cycles are two fundamental biogeophysical processes in the biosphere (Law et al., 2002). As the initial carbon fixed by vegetation through photosynthesis, terrestrial gross primary productivity (GPP) is a primary driver of the global carbon cycle (Running et al., 2004; Anav et al., 2015). GPP also regulates basic ecosystem functions, such as respiration and growth, and provides the total carbohydrate matter to sustain the food web, which directly contributes to human welfare (Beer et al., 2010; Running, 2012). As a vital component of the water cycle, evapotranspiration (ET) is the sum of plant transpiration, soil evaporation and canopy interception (Mu et al., 2007; Sun et al., 2011a; Fang et al., 2015). ET

* Corresponding authors at: Department of Geography, University of North Carolina at Chapel Hill, Chapel Hill 27599, NC, USA.
E-mail addresses: ylzhang@unc.edu (Y. Zhang), csong@email.unc.edu (C. Song).

http://dx.doi.org/10.1016/j.agrformet.2016.04.003
0168-1923/

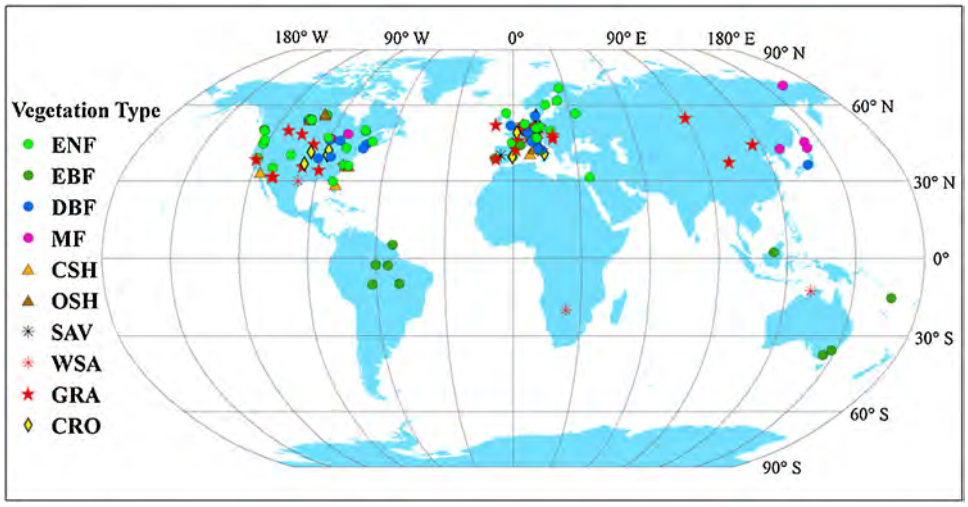

Fig. 1. FLUXNET tower sites used in this study. Biomes include evergreen needle-leaf forest (ENF), evergreen broad-leaf forest (EBF), deciduous broad-leaf forest (DBF), mixed forest (MF), closed shrub (CSH), open shrub (OSH), savannas (SAV), woody savannas (WSA), grassland (GRA), and cropland (CRO). (For interpretation of the references to colour in this figure legend, the reader is referred to the web version of this article.)

not only controls soil moisture and catchment water yield (Bosch and Hewlett, 1982; Sun et al., 2011a,b), but also affects regional precipitation patterns due to its feedback to the climate system (Koster et al., 2004; Seneviratne et al., 2006). Accurately estimating spatial and temporal distributions of GPP and ET are critical to understand ecosystem functions and their responses to global environmental changes, such as human-induced climate warming and land use change (McGuire et al., 2001; Tian et al., 2010).

Carbon and water fluxes are inherently coupled on multiple scales (Law et al., 2002; Waring and Running 2010; Sun et al., 2011b). From leaf to stand and ecosystem levels, carbon gains through photosynthesis and water losses through transpiration are mainly regulated by plant stomatal behavior in response to a set of environmental conditions (Jarvis, 1976). The ratio of GPP over ET, defined as the water use efficiency (WUE), is an essential quantity that characterizes complex trade-offs between carbon gain and water loss (Ponton et al., 2006; Waring and Running, 2010). Thus, between GPP and ET, knowing one provides information to estimate the other given WUE, providing an efficient way to integrate GPP and ET into simplified eco-hydrological models (Sun et al., 2011a,b). Methodologically, those models that independently estimate ET and then use ET or ET-inferred water stress to estimate GPP can be regarded as water-centric models. For example, Beer et al. (2010) used the water-centric approach to estimate global GPP based on basin-scaled ET and WUE. Sun et al. (2011b) developed the WaSSI model in which they first estimated ET with an empirical model, and then estimated GPP based on WUE. Other models, such as CASA (Potter et al., 1993), 3 PG (Landsberg and Waring, 1997; Nole et al., 2009), TECO (Weng and Luo, 2008), and EC-LUE (Yuan et al., 2010), used a soil moisture sub-model or a Penman-Monteith equation to independently estimate ET, and then use ET-related water stress to estimate GPP. However, ET is still the least quantifiable component of water cycle at all scales due to the challenge in characterizing large sets of controlling factors, including climate, plant biophysics, soil properties, and topography (Mu et al., 2007; Sun et al., 2011a,b; Wang and Dickinson, 2012; Wilson et al., 2001). Thus, water-centric models that use ET to estimate GPP can have large predictive errors.

Compared to ET, GPP has been more readily estimated with remotely sensed-based models, such as light-use efficiency (LUE) models (Potter et al., 1993; Running et al., 2004; Song et al., 2013; Yuan et al., 2007; Zhao and Running, 2010). LUE is a key biophysical parameter, quantifying the capacity of plants to convert absorbed light to carbohydrate through photosynthesis (Monteith, 1972). GPP models based on LUE using remotely sensed data from space-borne satellites are considered to have high potential to adequately capture the spatial-temporal dynamics of GPP on the global scale due to its simplicity and the solid biophysical basis (Running et al., 2004; Song et al., 2013). Although numerous LUE-based GPP models have been developed, they have rarely been coupled with the estimation of ET (Hu et al., 2013). Recent studies showed that the coupling of GPP and ET in terms of WUE may be further regulated by the linear or non-linear effects of vapor pressure deficit (VPD), corresponding to the inherent WUE (IWUE) (Beer et al., 2009) or underlying WUE (UWUE) (Zhou et al., 2014), respectively. With appropriate WUE, LUE-based GPP model potentially provides a new and effective pathway to estimate ET, which can be referred to as a carbon-centric model.

The objective of this study is to develop a monthly coupled carbon and water (CCW) model that first estimates GPP based on LUE theory and then estimates ET based on WUE theory. We intend to develop CCW as a tool that is computationally simple, yet provides GPP and ET estimates with comparable accuracy to more complex models that are currently in use. Such a carbon-centric model can be used to evaluate the impacts of land-use/land-cover change and climate change on GPP and ET at a wide range of scales. In CCW, we accounted for the effect of diffuse radiation on LUE. Diffuse radiation had been shown to be more efficiently used in photosynthesis by both theoretical and observational studies (Gu et al., 2002; King et al., 2011; Medlyn, 1998; Mercado et al., 2009; Turner et al., 2006b). However, most LUE models do not account for this effect (Yuan et al., 2014), potentially leading to underestimation of GPP. We evaluated two forms of GPP models: one considers Liebig's law, taking the more limiting factor between temperature and VPD (Yuan et al., 2007), and the other takes co-limiting effects of temperature and VPD on LUE simultaneously (Landsberg and Waring, 1997; Raich et al., 1991). We evaluated three water use efficiencies in estimating ET, including WUE, IWUE, and UWUE. We calibrated the CCW model parameters with global eddy covariance (EC) flux data from FLUXNET and remote sensing data from MODerate resolution Imaging Spectroradiometer (MODIS) from 2000 to 2007. The model performance was evaluated with reserved flux tower data that were not used in the model development. Finally, we used CCW to estimate global GPP and ET in 2001 and evaluated the model results with MODIS GPP and ET products as well as regional basin-scale ET derived from precipitation and stream flow data.

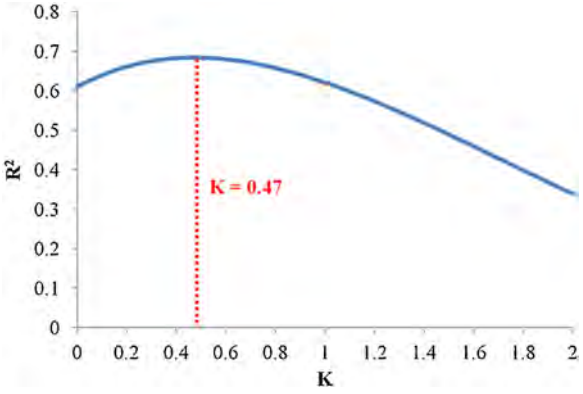

Fig. 2. The effect of the parameter *K* changes (Eq. (9)) on the coefficient of determination (R^2) between monthly observed ET and GPP × VPD^k for all biomes from the calibration dataset. R^2 was calculated with the intercept of the linear regression being forced to 0.

2. Methods and materials

2.1. Framework of coupled carbon and water (CCW) model

2.1.1. CCW GPP

In CCW, we estimated GPP as the product of absorbed photosynthetically active radiation (APAR) and realized LUE (ε) that is regulated by diffuse radiation, temperature and water stresses. We compared two GPP models (i.e., GPP_{OR} and GPP_{AND}):

$$GPP_{OR} = APAR \times \varepsilon = (PAR \times FPAR) \times \left(\varepsilon_{pot} \times R_s\right) \times \min(T_s, W_s) \quad (1)$$

$$GPP_{AND} = APAR \times \varepsilon = (PAR \times FPAR) \times \left(\varepsilon_{pot} \times R_s\right) \times (T_s \times W_s) \quad (2)$$

where PAR is the incident photosynthetically active radiation ($MJ\,m^{-2}$), which is assumed to be 45% of the short-wave total radiation in this study as in Running et al. (2000); FPAR is the fraction of PAR being absorbed by plants; ε_{pot} ($gC\,MJ^{-1}$) is the potential LUE realized by plants without environmental stresses; R_s, T_s and W_s are the environmental scalars related to diffuse radiation, temperature and water stresses, each of which takes value within the range of [0,1]; min() denotes the minimum value between T_s and W_s; GPP_{AND} is stressed by both T_s and W_s, while GPP_{OR} is only regulated by the more limiting factor from either T_s or W_s.

FPAR was found to have a linear relationship with the remote-sensing based normalized difference vegetation index (NDVI) (Myneni and Williams, 1994):

$$FPAR = a \times NDVI + b \quad (3)$$

where a and b are empirical parameters that are respectively set to 1.24 and −0.168 for MODIS NDVI according to Sims et al. (2005).

As the fraction of diffuse radiation in global radiation is always linked with the sky condition, we used a linear function of clear-sky index (CI), similar with the scalar in CFLUX model (Turner et al., 2006b; King et al., 2011), to quantify the effect of diffuse radiation on LUE:

$$R_s = 1 - K_1 \times CI \quad (4)$$

where K_1 is a biome-specific diffuse light response parameter; CI is defined as the ratio of actual radiation to clear-sky radiation. The calculation of clear-sky radiation is based on Raes et al. (2009). Given a specific sky condition, a smaller K_1 indicates a stronger influence of diffuse radiation on LUE.

T_s accounts for the non-linear effects of high and low temperatures on LUE, which was adopted from the TEM model (Raich et al., 1991):

$$T_s = \frac{(T - T_{min}) \times (T - T_{max})}{(T - T_{min}) \times (T - T_{max}) - \left(T - T_{opt}\right)^2} \quad (5)$$

where T is the monthly mean air temperature; T_{min}, T_{max} and T_{opt} are respectively the minimum, maximum and optimal air temperature for photosynthetic activity. T_s is set to 0 when T is lower than T_{min} or higher thanT_{max}. In this study,T_{opt} is a biome-dependent parameter, while T_{min} and T_{max} are set as −10 °C and 40 °C for all biomes, respectively.

Water stress plays an important role in regulating GPP, but modeling its effect is still far from satisfactory in current LUE models, largely due to the current inability of accurately estimating soil moisture over the whole root zone (Yuan et al., 2014; Zhang et al., 2015). Based on the global flux tower data, Zhang et al. (2015) comprehensively examined the effects of different moisture indicators on LUE along the soil-plant-atmosphere continuum, and found that VPD generally showed better association with LUE than precipitation and soil water content. Current MODIS GPP and ET algorithms also adopted VPD as moisture stress indictor. However, the constrains of VPD in their algorithms are both linear. In this study, we adopted a non-linear vapor pressure scalar similar to the canopy conductance scalar used in the 3 PG model (Landsberg and Waring, 1997):

$$W_s = \exp(-K_2 \times (VPD - VPD_{min})) \quad (6)$$

where VPD is the monthly vapor pressure deficit (VPD, hPa); K_2 is a biome-specific moisture sensitivity parameter. A higherK_2 indicates a larger reduction of LUE in response to VPD. VPD_{min} is the minimum VPD exceeding which moisture stress starts to take effect. W_s is set to 1 when VPD is lower thanVPD_{min}. In this study, VPD_{min} is set as 5 hPa for all biomes. In this paper, we used the monthly mean daily VPD as a substitute of the effective daytime VPD to constrain GPP as well as ET shown below, because we found that at the monthly scale, daily averaged VPD is highly linearly correlated with daytime VPD ($R^2 = 0.98$, $P < 0.001$; Fig. S1).

The model parameters mentioned above, including ε_{pot}, K_1, T_{opt} and K_2 for GPP_{OR} and GPP_{AND}, were calibrated based on the global FLUXNET data. The process is presented in Section 2.2.2.

2.1.2. CCW ET

In CCW, we examined ET estimated from GPP based on three different definitions of water use efficiencies as:

$$WUE = \frac{GPP}{ET} \quad (7)$$

$$IWUE = \frac{GPP \times VPD}{ET} \quad (8)$$

$$UWUE = \frac{GPP \times VPD^K}{ET} \quad (9)$$

where WUE, IWUE and UWUE represents standard WUE (Ponton et al., 2006), inherent WUE (Beer et al., 2009) and underlying WUE (Zhou et al., 2014), respectively. ET can be estimated by solving Eqs. (7)–(9), denoted as ET_{WUE}, ET_{IWUE} and ET_{UWUE}, respectively. K in Eq. (9) is a parameter for UWUE. UWUE is equivalent to IWUE when K equals 1, and equivalent to WUE when K equals 0. In this study, we estimated K and all three biome-dependent WUEs based on the global FLUXNET data. The details are given in Section 2.2.2. Conceptually, compared to ET_{WUE}, ET_{IWUE} and ET_{UWUE} further account for the linear and non-linear effects of VPD on GPP-ET coupling, respectively.

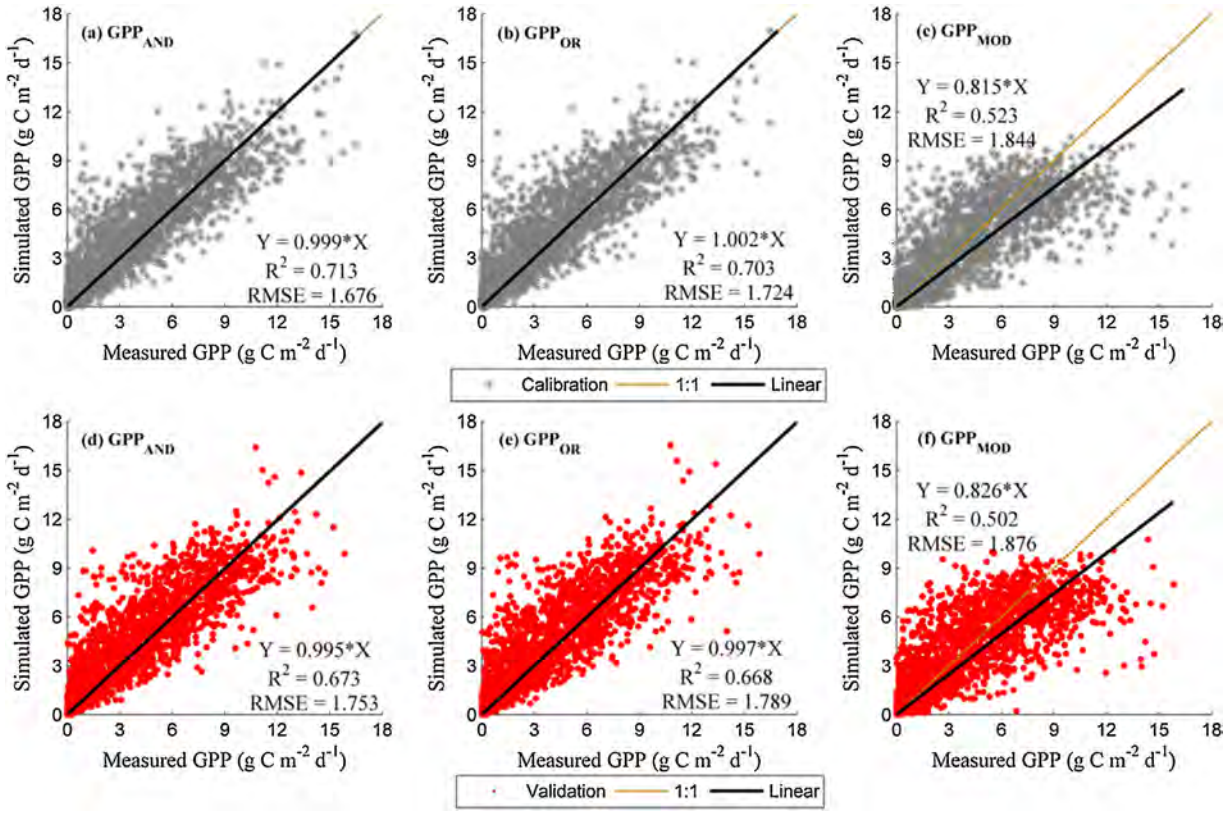

Fig. 3. Evaluation of GPP estimated by CCW with flux-tower derived GPP for all biomes. In CCW, GPP_{AND} (a, d) accounts for the co-limitation of temperature and VPD, while GPP_{OR} (b, e) accounts for the minimum limitation of temperature and VPD. GPP_{MOD} (c, f) is MODIS GPP product (MOD17). The gray and red colors represent calibration and validation datasets, respectively. The brown dotted line is the 1:1 line. The black line is the linear fit for all plots with intercept forced to 0. (For interpretation of the references to colour in this figure legend, the reader is referred to the web version of this article.)

2.2. Model calibration and validation

2.2.1. Global site-level data

The site-level data used to calibrate and evaluate CCW were composed of EC flux dataset from FLUXNET during 2000–2007, including monthly mean daily GPP, ET, global radiation, air temperature and VPD, and MODIS NDVI over the pixels where the flux towers are located. One should note that unlike ET (or latent heat), GPP is not a directly measured quantity, but derived from the difference between measured net ecosystem exchange (NEE) and estimated ecosystem respiration (Reichstein et al., 2005). For convenience, we still refer to GPP derived from flux tower as "observed" data. The FLUXNET dataset integrates global observations of carbon, water and energy fluxes over 253 EC flux towers (http://www.fluxdata.org/). These towers span latitudes from 70° N to 37° S, covering a wide range of climatic zones and terrestrial ecosystems. In the FLUXNET, the daily data was integrated from gap-filled half-hour data and then subsequently aggregated into monthly means. We excluded the data when the monthly averaged daily gap filling ratio was higher than 15%. Some extreme records with monthly LUE higher than 3.0 g C MJ^{-1} or WUE higher than 6.0 g C kg^{-1} H_2O were also removed. Finally, we dropped sites with total monthly records less than one year. After data screening, 142 EC flux towers (Table S1) distributed across 10 biomes totaling 4185 monthly records were selected (Fig. 1; Table 1). These biomes include evergreen needle-leaf forest (ENF), evergreen broad-leaf forest (EBF), deciduous broad-leaf forest (DBF), mixed forest (MF), closed shrub (CSH), open shrub (OSH), savannas (SAV), woody savannas (WSA), grassland (GRA), and cropland (CRO).

Table 1
Data usage in validation and calibration groups for different biomes. Biome abbreviations are given in Fig. 1. Please note that validation and calibration records do not precisely match the 1:1 ratio due to the random variation in sampling.

Biome	No. of Sites	Total Records	ValidationRecords	CalibrationRecords
ENF	46	1555	807	748
EBF	13	397	183	214
DBF	17	556	276	280
MF	8	175	88	87
CSH	5	156	77	79
OSH	5	93	44	49
SAV	1	30	17	13
WSA	5	163	83	80
GRA	28	744	347	397
CRO	14	316	178	138
Total	142	4185	2100	2085

The NDVI data for each tower site were derived from the monthly $1 \times 1\,km^2$ MODIS product (i.e., MOD13A3C5). These data were obtained from the Oak Ridge National Laboratory Archive Center (http://daac.ornl.gov/MODIS/MODIS-menu/modis_webservice.html). We used the single pixel in which the tower is located instead of the conventional N × N pixel window (N is usually set to 3, 5 or a larger value). We recognized there is potential geo-location error for MODIS pixels, but the footprint size of the flux tower (a few hundred meters to 1 km) is usually smaller than the $1 \times 1\,km^2$ MODIS pixel. The N × N pixel window would cover an area that is often too large to represent the spatial extent of a flux tower and may produce systematic bias, which is especially obvious for the towers located in complex terrain (Xiao et al., 2004). To minimize the effects from cloud contaminations, cloud shadows

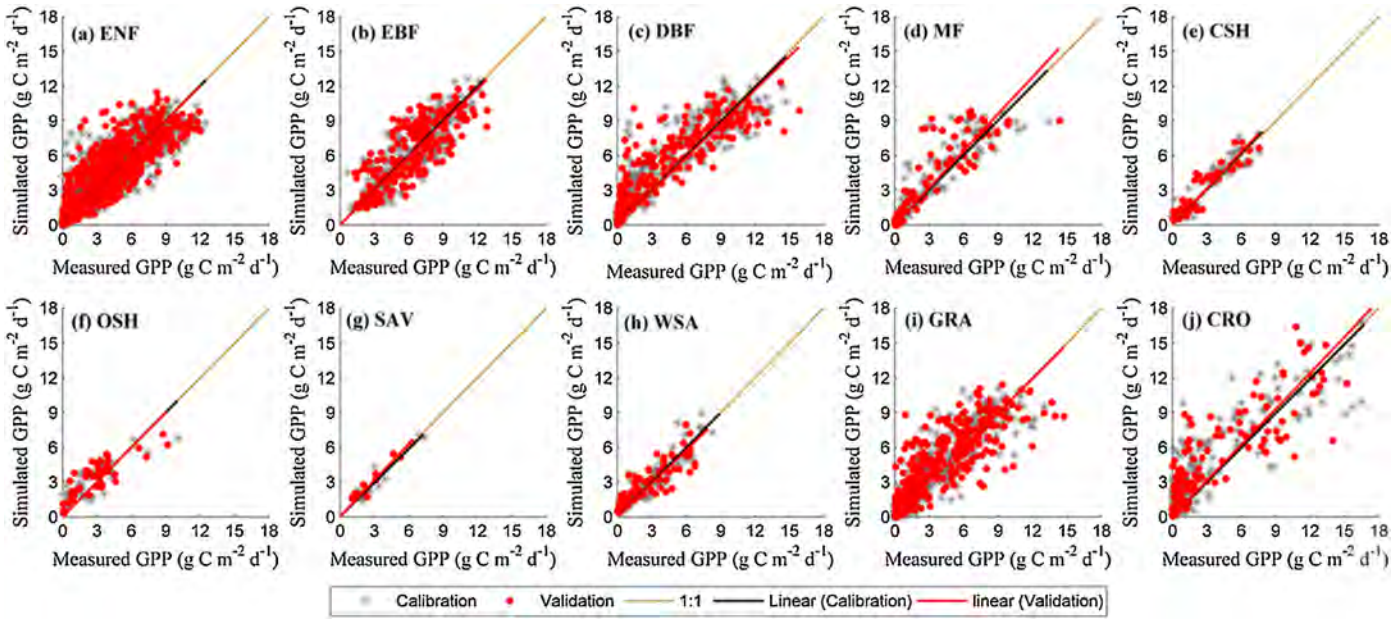

Fig. 4. Evaluations of GPP estimated by CCW (i.e. GPP_{AND} in Eq. (2)) with flux-tower derived GPP for different biomes. The gray and red colors represent calibration and validation datasets, respectively. The biome abbreviations are given in Fig. 1. The brown dotted line is the 1:1 line. The black and red lines are the linear fits with the intercept forced to 0 for calibration and validation datasets, respectively. The statistics including linear slope, R^2 and RMSE for each biome are given in Table S2. (For interpretation of the references to colour in this figure legend, the reader is referred to the web version of this article.)

and aerosols, we smoothed the monthly NDVI data for each site using a double logistic method based on the pixel quality flag in the software package of TIMSAT 3.1 (Jönsson and Eklundh, 2004).

2.2.2. Calibration and validation

We randomly split the monthly records for each flux site at a 1:1 ratio for calibration and validation groups (Table 1). The calibration dataset was used to estimate the parameters for the two GPP models (i.e., biome-specific ε_{pot}, K_1, T_{opt} and K_2) through Monte Carlo simulation and derive parameters for three ET models (i.e., K and biome-specific WUEs) using a statistical method. Please note that the calibration is based on the unit of "biome", but not "single site". Given the limited EC tower sites (Table 1), the data split on each site could ensure the calibration process cover enough variations of EC data within the biome, while make the validation process hold necessary data variations to test the model.

The key logic of the Monte Carlo simulation is to repeat random sampling within given parameter ranges, and then identify optimal parameters by comparing model outputs with reference data in all simulations (Wang et al., 1995). The agreement between the simulated and observed data is usually quantified by the coefficient of determination (R^2), root mean squared error (RMSE), or Nash-Sutcliffe Efficiency (NSE) (Janssen and Heuberger, 1995). However, each of these criteria carries some flaws. For example, R^2 could not expose systematic overestimation or underestimation by the model. The scatter between observed and simulated data could result in a high R^2, even when the prediction is bad with the slope far from the unit and the intercept not equal 0. Since both RMSE and NSE are calculated based on the squared differences between observed and simulated data, they are rather sensitive to outliers or extreme values (Janssen and Heuberger, 1995; Krause et al., 2005). In addition, similar to R^2, NSE is also not very sensitive to systematic model over- or underestimation, especially when the observed values are low (Krause et al., 2005). In this study, we adopted the weighted R^2 (wR^2) to overcome these problems (Krause et al., 2005), and regarded it as the performance indicator for the Monte Carlo simulation:

$$wR^2 = \begin{cases} |b| \times R^2 & b < 1 \\ |b|^{-1} \times R^2 & b \geq 1 \end{cases} \quad (10)$$

where || takes the absolute value; b and R^2 are the slope and coefficient of determination for the regression when the intercept is forced to be 0 (Chatterjee and Hadi, 1986). $wR^2 = 1$ indicates a perfect match between simulated and observed data.

We conducted the Monte Carlo simulations to calibrate parameters for GPP_{OR} and GPP_{AND} for each biome following the steps from Hu et al. (2009). First, we established a broad range for each parameter based on prior knowledge (i.e., ε_{pot}: 0–3.5, K_1: 0–1, T_{opt}:15–30, K_2:0–0.4). Then we performed 100,000 Monte Carlo simulations with the parameters randomly selected within the given ranges. In each simulation, we calculated wR^2 for its parameter set based on the simulated and observed GPP. Third, we narrowed the parameter range set based on the statistics from the top 100 simulations with the highest wR^2. We then conducted the above simulations again using the updated parameter ranges. After the 100,000 simulations, we selected the best-fit parameter set with the highest wR^2 for each biome. The biome-specific calibrated parameters for GPP_{AND} are shown in Table 2.

For UWUE (Eq. (9)), we examined the influences of K changes on the correlation between monthly ET and $GPP \times VPD^k$ for all biomes, and identified K as 0.47 to best describe the nonlinear effect of VPD on carbon-water coupling (Fig. 2). Based on the calibration data, we derived WUE, IWUE and UWUE for each biome using linear regression (Table 3). For example, we first generate a scatter plot with X-axis being ET and Y-axis being $GPP \times VPD^{0.47}$, and linearly fit them by forcing the intercept to 0. The slope of the linear regression is UWUE.

Based on the validation data, we evaluated the performances of GPP_{AND} and GPP_{OR} for all biomes in terms of slope, R^2, and RMSE of the linear regression with the intercept forced to zero. We then selected the model that provided a more accurate estimate of GPP to estimate ET. Next, we compared three ET models

Table 2
Biome-specific calibrated parameters for GPP_{AND}, which is co-limited by temperature and VPD, through the Monte Carlo simulation. We set $T_{min} = -10.0\,^{\circ}C$, $T_{max} = 40.0\,^{\circ}C$ and $VPD_{min} = 5.0$hPa for all biomes. Biome abbreviations are given in Fig. 1.

Biome	ε_{pot}(g C m−2)	K_1	T_{pot}(°C)	K_2
ENF	2.516	0.575	27.8	0.091
EBF	2.892	0.745	28.0	0.050
DBF	2.233	0.550	28.0	0.032
MF	2.758	0.755	27.7	0.053
CSH	2.209	0.643	26.7	0.095
OSH	2.144	0.789	27.9	0.057
SAV	1.897	0.302	25.0	0.046
WSA	2.190	0.643	26.7	0.032
GRA	2.397	0.665	16.9	0.088
CRO	2.319	0.254	28.0	0.096

(i.e., ET_{WUE}, ET_{IWUE} and ET_{UWUE}) for all biomes and chose the most accurate model for CCW. During this process, we used the site-level MODIS GPP and MODIS ET products to evaluate the performance of CCW. MODIS GPP was estimated through a LUE model, which accounted for the limitations of cold temperature and water stress in terms of day-time VPD, but not for the effect of diffuse radiation (Zhao and Running, 2010). MODIS ET was calculated based on the Penman-Monteith equation, fully considering the canopy transpiration and evaporation from the soil and rain water interception (Mu et al., 2011). As the first routinely satellite-driven datasets at a moderate spatial resolution (i.e. 1 × 1 km) and temporal resolution (i.e., 8 day), MODIS GPP and ET products have been widely used to monitor global vegetation functions. The pixel values of MODIS GPP and ET for each tower site from 2000 to 2007 were extracted from the 1 × 1 km monthly MODIS products (i.e., MOD17A2 and MOD16A2C5.5), which were downloaded from the NTSG website (http://www.ntsg.umt.edu/). We further evaluated the performance of CCW for each biome based on the tower-level observed data. In addition, we used the Taylor diagram to evaluate the performances of CCW across different flux tower sites. A Taylor diagram provides a graphical summary on how close a pattern (or a set of patterns) matches observations in a single polar coordinate (Taylor, 2001). The similarity between two patterns is quantified in terms of their correlation, centered root mean square difference and the amplitude of their variations.

2.3. Estimating global GPP and ET with CCW

After we identified the final models for GPP and ET, we used CCW to estimate global GPP and ET at a spatial resolution of 0.05° × 0.05° for the year 2001. We chose the year 2001 because MODIS GPP and ET products (C5.5) used for evaluation in this study were produced with a static 2001 land cover (http://www.ntsg.umt.edu/project/mod17). The global dataset used here includes 0.05° × 0.05° MODIS land cover data (MOD12C1 V4; consistent with MODIS GPP and ET products), monthly 0.05° × 0.05° MODIS NDVI data (MOD13C2 V5), and monthly 0.5° × 0.5 °CRU-NCEP (V5) climate data in 2001. The CRU-NCEP climate data are the combination of two existing global climatic datasets: ground observation-based CRU TS 3.2 and model-based NCEP-NCAR Reanalysis data, which had been widely used in global change studies (Hashimoto et al., 2013; Le Quéré et al., 2009; Wang et al., 2013). We downloaded the 6-hourly CRU-NCEP V5 datasets including global radiation, precipitation, air temperature, air pressure and air specific humidity from the ftp site (http://dods.extra.cea.fr/data/p529viov/cruncep/V5_1901_2013/). The 6-hourly data were further aggregated into monthly data. Given that the CRU-NCEP data did not include VPD, we calculated VPD using monthly air temperature, atmospheric pressure and air specific humidity from CRU-NCEP (Castellvi et al., 1996). To match the spatial resolution of the MODIS data, we generated the 0.05° × 0.05 °Climate data from the coarse CRU-NCEP data with bilinear interpolation. As we lack flux data for deciduous needleleaf forest (DNF), we used the parameters from MF as a substitute based on Zhao and Running (2010), who showed similar GPP model parameters between DNF and MF. To evaluate the CCW modeling results at the global scale, we downloaded the 0.05° × 0.05°annual MODIS GPP and ET products (C5.5) in 2001 from the NTSG website (http://www.ntsg.umt.edu/). To further evaluate annual ET estimated by CCW on the regional scale, we obtained the multi-year averaged (1990–2009) precipitation (P) and measured stream flow (Q) data at 421 U.S. Geological Survey (USGS) gauged reference watersheds (http://waterdata.usgs.gov/nwis/rt). The multi-year averaged precipitation for each watershed is derived from 4 × 4 km resolution PRISM data (http://www.prism.oregonstate.edu/).

3. Results

3.1. Evaluation of modeled GPP

We evaluated two GPP models (i.e., GPP_{OR} and GPP_{AND}) for all biomes based on flux tower-derived GPP (Fig. 3). We found that GPP_{AND} showed slightly better performances in matching tower-based GPP than GPP_{OR} by all measures. For the calibration dataset, GPP_{AND} explained 71.3% of the variations of tower-based GPP (Fig. 3a), while GPP_{OR} explained 70.3% of the variations (Fig. 3b). Similarly, GPP_{AND} explained slightly higher variations of tower-based GPP ($R^2 = 0.673$, $P < 0.01$) than GPP_{OR} ($R^2 = 0.668$, $P < 0.01$) for the validation dataset (Fig. 3e and f). In addition, GPP_{AND} showed slightly lower RMSE with tower-based GPP than GPP_{OR} both for calibration and validation datasets. Overall, Neither GPP_{AND} nor

Table 3
Biome-specific ecosystem water-use efficiency (WUE; g C kg^{-1} H_2O), inherent water-use efficiency (IWUE; g C hPa^{-1} kg^{-1} H_2O) and underlying water-use efficiency (UWUE; g C $hPa^{-0.47}$ kg^{-1} H_2O) used for ET estimation. The slope (i.e., WUEs) and R^2 were estimated from calibration data for each biome by forcing the intercept of the linear regression to be 0. Biome abbreviations are given in Fig. 1.

Biome	WUE	(ET vs GPP)	IWUE	(ET vs GPP × VPD)	UWUE	(ET vs GPP × $VPD^{0.47}$)
	Slope	R^2	Slope	R^2	Slope	R^2
ENF	2.710	0.566	16.665	0.579	6.210	0.635
EBF	2.675	0.640	19.074	0.564	6.587	0.750
DBF	3.280	0.775	23.608	0.754	8.122	0.815
MF	3.349	0.675	15.685	0.505	6.711	0.641
CSH	1.734	0.568	13.727	0.602	4.525	0.627
OSH	1.679	0.735	12.103	0.708	4.223	0.737
SAV	2.032	0.750	20.609	0.524	5.720	0.921
WSA	1.689	0.830	19.370	0.545	5.214	0.778
GRA	2.333	0.614	14.718	0.672	5.378	0.729
CRO	2.533	0.599	16.630	0.635	6.032	0.648
All	2.595	0.611	17.465	0.621	6.196	0.684

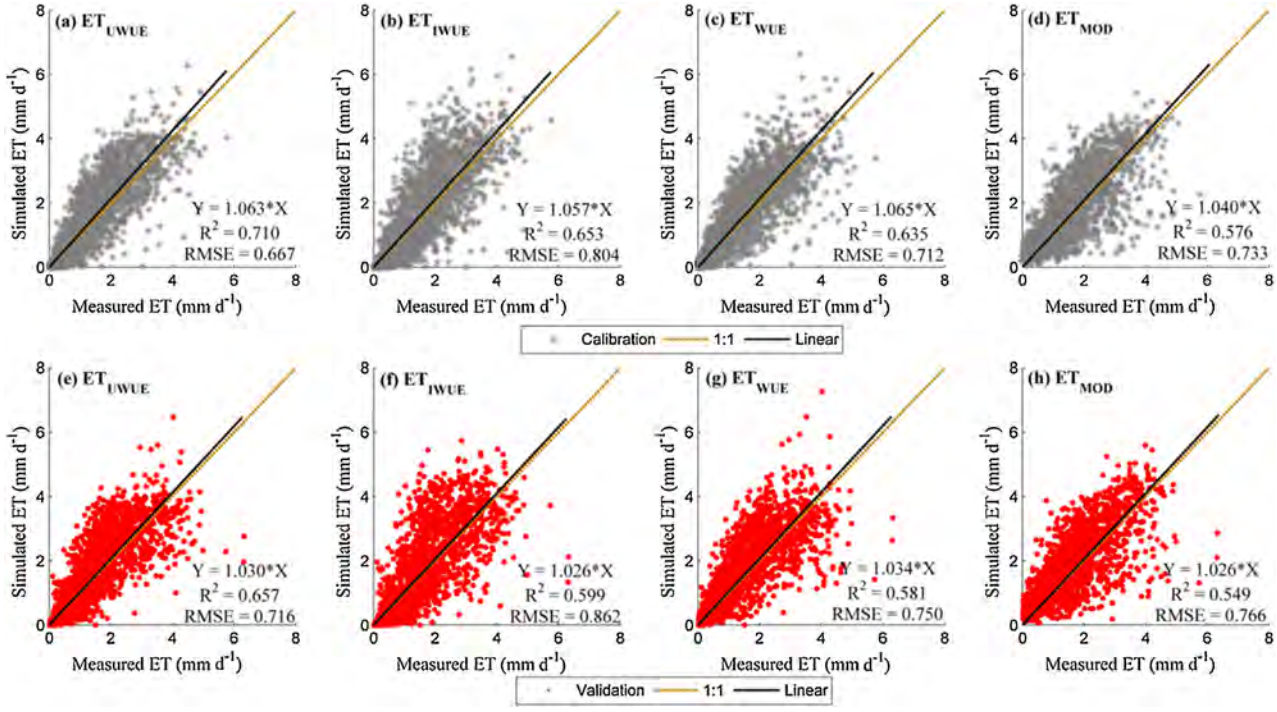

Fig. 5. Evaluations of ET estimated by CCW with flux-tower derived ET for all biomes. ET_{UWUE} (a, e), ET_{IWUE} (b, f) and ET_{WUE} (c, g) are calculated using the concepts of UWUE, IWUE and WUE in CCW, respectively. ET_{MOD} (d, h) is MODIS ET product (MOD16). The gray and red colors represent calibration and validation datasets, respectively. The brown dotted line is the 1:1 line. The black line is the linear fit for all plots with intercept forced to 0. (For interpretation of the references to colour in this figure legend, the reader is referred to the web version of this article.)

GPP_{OR} showed any systematic errors (i.e., slope ≈ 1.00) with tower-based GPP across all biomes. However, as the reference data for CCW, GPP_{MOD} generally underestimated GPP derived from the flux towers, especially for higher GPP values (slope = 0.815–0.826, R^2 = 0.502–0.523; Fig. 3c and f).

We further evaluated GPP_{AND} for different biomes based on flux tower-derived GPP. GPP_{AND} showed essentially unbiased estimation of GPP with a linear slope close to one for most biomes in the calibration dataset, which further determined the performances of GPP_{AND} in the validation dataset (Fig. 4; Table S2). GPP_{AND} captured over 85% of the variations of tower-derived GPP for SAV and CSH from validation dataset, and over 65% of the variations for MF, DBF and ENF (Table S2). However, GPP_{AND} generally explained lower variations (<40%) of tower-based GPP for OSH. GPP_{AND} tended to overestimate GPP for MF (Fig. 4d) and CRO (Fig. 4j), but underestimate GPP for some GRA (Fig. 4i), OSH (Fig. 4j) and DBF (Fig. 4c) sites.

3.2. Evaluation of modeled ET

As GPP_{AND} showed a slightly better performance than GPP_{OR}, we chose GPP_{AND} as the GPP model in CCW and estimated different WUE-based ETs (i.e. ET_{WUE}, ET_{IWUE}, and ET_{IWUE}). We found that ET_{UWUE} showed the best performance in simulating ET among the three ET models in terms of R^2 and RMSE with tower-derived ET across all biomes (Fig. 5). Overall, all three ET models estimated ET that matched with tower-based ET slightly better in the calibration dataset than that in the validation dataset. Based on the validation dataset, ET_{UWUE} explained 65.7% of the variations of tower-measured ET for all biomes (Fig. 5e), followed by ET_{IWUE} (59.9%; Fig. 5f) and ET_{WUE} (58.1%; Fig. 5g). There were small systematic overestimations for all the three forms of ET, with the largest overestimation occurring in ET_{WUE} (3.4%; Fig. 5g) and lowest in ET_{IWUE} (2.6%; Fig. 5f). ET_{UWUE} showed moderate systematic overestimation (3.0%; Fig. 5e), but it had the smallest RMSE (0.716 mm d^{-1}). As the reference data for CCW, MODIS ET generally matched the tower-measured ET well with the linear slope lower than 3% for validation dataset (Fig. 5d and h). However, ET_{MOD} explained about 55% of the variations of tower-measured ET for all biomes, which was lower than CCW ETs, especially ET_{UWUE}.

We further evaluated ET_{UWUE} for different biomes based on tower-measured ET. ET_{UWUE} generally matched well with tower-based ET for most biomes, and there were no significant differences in predicted ET between the calibration and validation datasets (Fig. 6; Table S3). Based on the validation dataset, ET_{UWUE} explained over 70% of the variations in tower-measured ET for half of the biomes, especially for SAV (R^2 = 0.930, $P < 0.01$). However, ET_{UWUE} generally predicted ET poorly in CSH (R^2 = 42.3%, $P < 0.01$), EBF (R^2 = 45.8%, $P < 0.01$) and ENF (R^2 = 54.2%, $P < 0.01$). Overall, ET_{UWUE} showed almost no systematic errors (i.e. |slope-1| < 5%) with tower-based ET in half of the biomes. However, ET_{UWUE} tended to underestimate ET for WSA, and overestimate ET for MF, OSH and CRO (Fig. 6; Table S3), reflecting the model uncertainties over different biomes.

3.3. Model evaluation at the site level

Based on the above analysis, we chose GPP_{AND} and ET_{UWUE} as the predictive models of GPP and ET in CCW, respectively. The environmental scalar functions used in CCW for diffuse radiation, temperature, and water stress on optimal LUE generally matched – the observed response curves of realized LUE, i.e., the linear response of LUE to CI (Fig. 7a and b), bell-shaped curves of LUE to air temperature (Fig. 7c and d), and exponential response of LUE to VPD (Fig. 7e and f). The linearity of response of LUE to CI was obvious in most biomes, especially in ENF, EBF and CSH (Fig. 7a). However, DBF and CRO showed relatively poor linearity of CI responses (Fig. 7a), probably due to the larger site variations in canopy structures or plant function types (e.g. C3/C4 for CRO). Overall, most biomes showed convergent responses to environ-

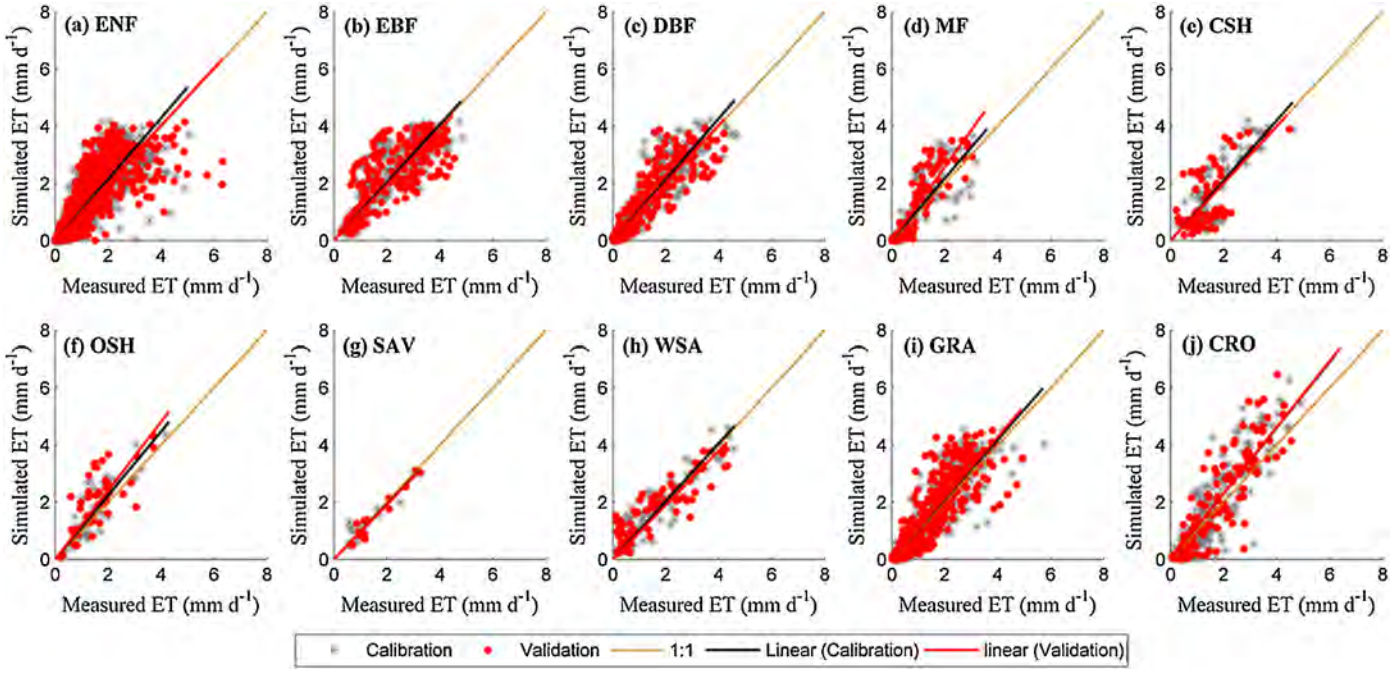

Fig. 6. Evaluations of ET estimated by CCW (i.e., ET_{UWUE}) with flux-tower derived GPP for different biomes. The gray and red colors represent the calibration and validation datasets, respectively. The biome abbreviations are given in Fig. 1. The brown dot line is the 1:1 line. The black and red lines are the linear fits with the intercept forced to 0 for the calibration and validation datasets, respectively. The statistics including linear slope, R^2 and RMSE for each biome are given in Table S3. (For interpretation of the references to colour in this figure legend, the reader is referred to the web version of this article.)

mental factors although they had different optimal LUEs. The large within-biome co-variation between each factor and LUE in Fig. 7a,c and e was probably related to the influences of other uncontrolled environmental factors on the observed LUE. To examine the sensitivity of CCW to its parameters, we conducted an analysis on the influence of parameter change on model performance in terms of wR^2. We calculated wR^2 for each biome based on the calibration dataset when only one parameter in CCW changed while all the other parameters were held at the optimal values. Using ENF as an example (Fig. 8), we found that CCW GPP was generally most sensitive to variations in ε_{opt} and K_1, moderately sensitive to T_{opt} and K_2, and least sensitive to VPD_{min}, T_{max} and T_{min}. In this study, VPD_{min}, T_{max} and T_{min} were set as constants for all biomes, which generally matched the observed thresholds (Fig. 7a, c and e). CCW ET seemed to be equally sensitive to variation in K and $UWUE$. Other biomes generally showed the similar model sensitivity with ENF except SAV and WSA (Table S4). These two biomes, which are mainly distributed in arid areas, were found to be most sensitive to the variation in K_2 in estimating GPP.

We further evaluated the performances of CCW in predicting GPP and ET at the site scale based on the validation dataset. These results were summarized in the Taylor diagrams (Taylor, 2001) (Fig. 9). Overall, CCW simulated GPP better than ET for most sites, although the model performances for GPP and ET were both quite variable across sites (Fig. 9). In the Taylor diagram for predicted GPP (Fig. 9a), 77% of the sites showed the correlation higher than 0.7, and normalized RMSE less than 0.75, while only 62% of the sites showed the same statistics in the ET diagram (Fig. 9b). GPP showed poor performances in some evergreen and mixed forest sites with large normalized RMSE (e.g., A1–A4 in Fig. 9a), and the errors were further propagated into ET estimation (e.g., A1–A4 in Fig. 9b).

3.4. Modeled global GPP and ET

We estimated global GPP and ET by CCW based on MODIS and CRU-NCEP climate data at a spatial resolution of $0.05^\circ \times 0.05^\circ$ for the year 2001 (Fig. 10). Annual GPP estimated by CCW showed high values (i.e., $> 3000\,g\,C\,m^{-2}\,yr^{-1}$) in tropical zones, especially in the Amazon, Congo, and Asian tropical rainforests, and low values (i.e., $< 500\,g\,C\,m^{-2}\,yr^{-1}$) in arid, semiarid and arctic zones (e.g., central Australia, southwestern USA, northern Russia and Canada). Temperate and subtropical zones (e.g., western Europe, and southeastern USA and China) showed moderate values (i.e., $1000 \sim 2500\,g\,C\,m^{-2}\,yr^{-1}$). Annual ET estimated by CCW generally showed similar spatial pattern with GPP (Fig. 10). However, higher ET (i.e., $> 1000\,mm\,yr^{-1}$) spanned both the central tropical and southern tropical regions.

Annual global GPP estimated by CCW over vegetated areas was $1229 \pm 911\,g\,C\,m^{-2}\,yr^{-1}$ (or $134.2\,Pg\,C\,yr^{-1}$) for the year 2001, 18.8% higher than MODIS GPP (i.e., $998 \pm 767\,g\,C\,m^{-2}\,yr^{-1}$ or $109.0\,Pg\,C\,yr^{-1}$), while global ET estimated by CCW was $522 \pm 369\,mm\,yr^{-1}$ (or $57.0 \times 10^3\,km^3$), nearly identical to MODIS ET ($554 \pm 374\,mm\,yr^{-1}$ or $60.5 \times 10^3\,km^3$), which was estimated with a much more complex algorithm (Mu et al., 2011). Global WUE estimated by CCW for the year 2001 was $2.35\,g\,C\,kg^{-1}\,H_2O$, that is close to the tower-derived WUE ($2.60\,g\,C\,kg^{-1}\,H_2O$; Table 3), but 24% higher than the WUE value estimated from MODIS products ($1.80\,g\,C\,kg^{-1}\,H_2O$). Global GPP and ET from CCW and MODIS over different biomes are presented in Fig. 11. Overall, CCW showed similar variations of GPP and ET among and within biomes with MODIS. However, GPP estimated by CCW was generally higher than MODIS for most biomes except CSH and OSH, while ET estimated by CCW was generally lower than MODIS except SAV, WSA and CRO.

4. Discussion

4.1. Model performance at the site scale

We evaluated the CCW performance by comparing modeled GPP and ET with those from flux tower measurements. Overall, GPP_{AND} showed a slightly better performance than GPP_{OR} (Fig. 3), probably because the combination of temperature and water stress produces

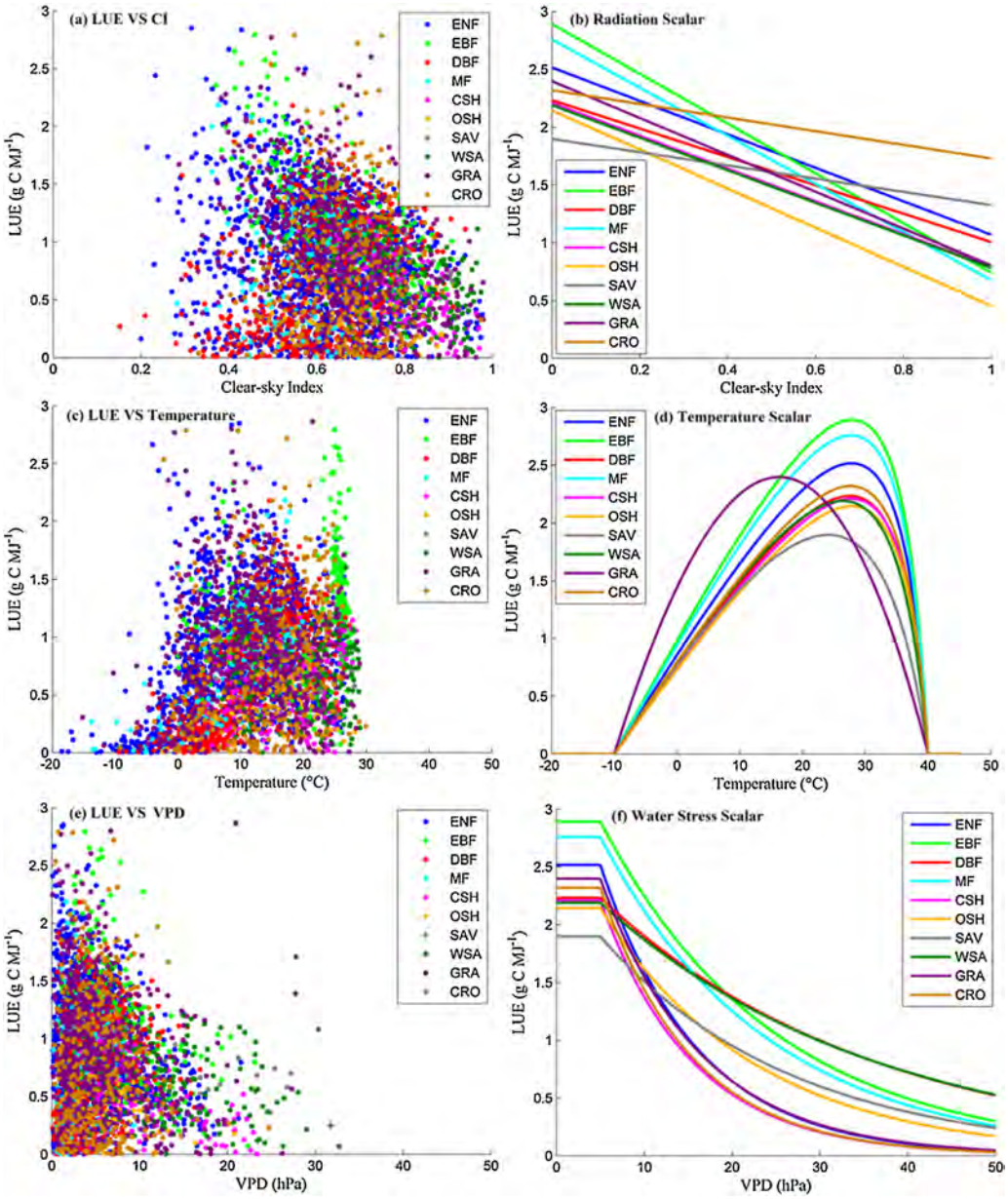

Fig. 7. Generalization of the different environmental controls on LUE in CCW. Sub-figure (a), (c) and (d) are scatter plots between realized LUE and clear-sky index, air temperature and vapor pressure deficit (VPD) on a monthly scale, respectively; (b), (d) and (f) are diffuse radiation (Eq. (4)), temperature (Eq. (5)) and water stress (Eq. (6)) scalars that regulate optimal LUE in CCW, respectively. The corresponding parameters for (b), (d) and (f) can be found in Table 2. Abbreviations for different biomes are given in Fig. 1. (For interpretation of the references to colour in this figure legend, the reader is referred to the web version of this article.)

more variations of constraints on LUE than a single factor, suggesting photosynthesis seems to be co-limited by environmental factors at the monthly scale. Diffuse radiation tends to increase LUE by penetrating the canopy and reaching the shaded leaves whose photosynthesis rates are light-limited (Gu et al., 2002; Turner et al., 2006b). However, few existing LUE models account for this phenomenon (Kanniah et al., 2012; King et al., 2011; Yuan et al., 2014). In this study, we confirmed the enhancement effect of diffuse radiation on LUE over different ecosystems (Fig. 7a), and incorporated it into CCW using a simple linear function of CI (shown in Eq. (4)). We showed that the optimal LUE for most biomes could decrease 50% to 80% (according to K_1 values in Table 2) from overcast to clear-sky conditions (Fig. 7b). The forest biomes (i.e., EBF and MF) generally showed higher sensitivity to sky condition than CRO and SAV biomes, reflecting the role of the heterogeneity of canopy structure in determining the response of LUE to diffuse radiation (Gu et al., 2002; Kanniah et al., 2012). The CRO biome was less sensitive to diffuse radiation probably due to the relatively uniform canopy structure and management practices (e.g., irrigation and fertilization). The ranges of potential LUE between overcast and clear-sky conditions in CCW generally covered the values derived from global flux tower data for those LUE models that did not account for the effect of diffuse radiation (Fig. 12). The CFLUX model used a scaled cloudiness index to quantify the diffuse radiation effect on LUE (King et al., 2011). The potential LUEs in CCW generally agreed with the values from CFLUX for most biomes, except DBF and shrub under overcast condition (Fig. 12). The differences in potential LUEs between CCW and CFLUX may be caused by the differences in model algorithms and data preparation processes. The clear-sky potential LUE for CRO in CCW was about 40% higher than the value used in MODIS GPP product (Zhao and Running, 2010). A recent study based on American Flux tower data also showed that MODIS GPP

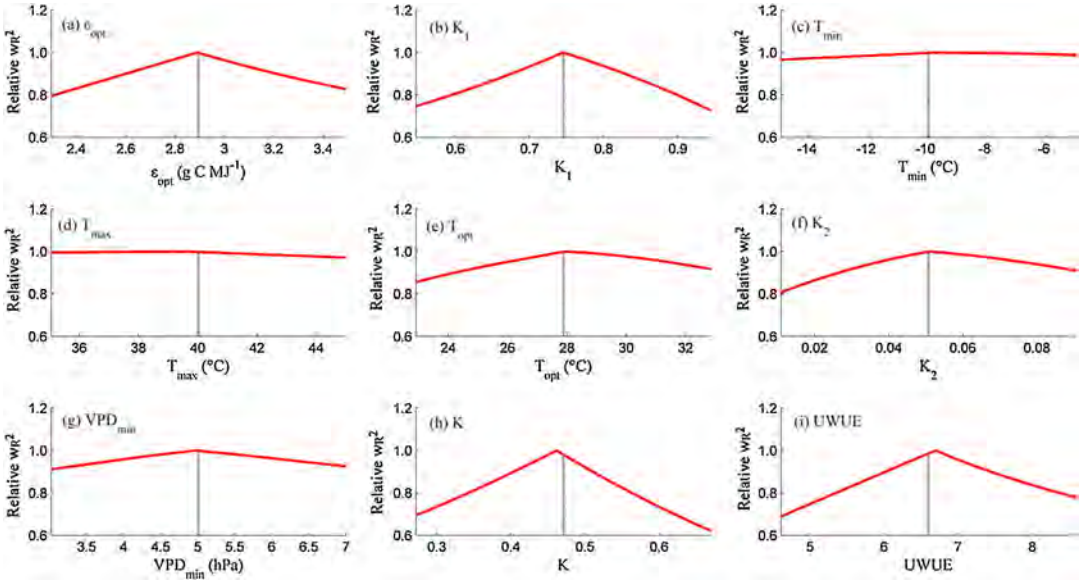

Fig. 8. Sensitivity of CCW to its model parameters for evergreen broadleaf forest (EBF) based on the calibration dataset. The vertical gray line indicates the optimal parameter used in CCW. The horizontal axis indicates the change in each parameter around its optimal value. The vertical axis refers to the relative wR^2 defined as the ratio of actual wR^2 for each changing parameter to the optimal wR^2. Sub-figure (a)–(g) indicate the changes of relative wR^2 for GPP; (h) and (i) indicate the changes of relative wR^2 for ET. The non-differentiation of the sensitivity curve around the optical parameter was largely due to the non-differentiable wR^2 defined in Eq. (10). K and UWUE did not produce the maximum wR^2 shown in other calibrated parameters because they were derived statistically (see Section 2.2.2).

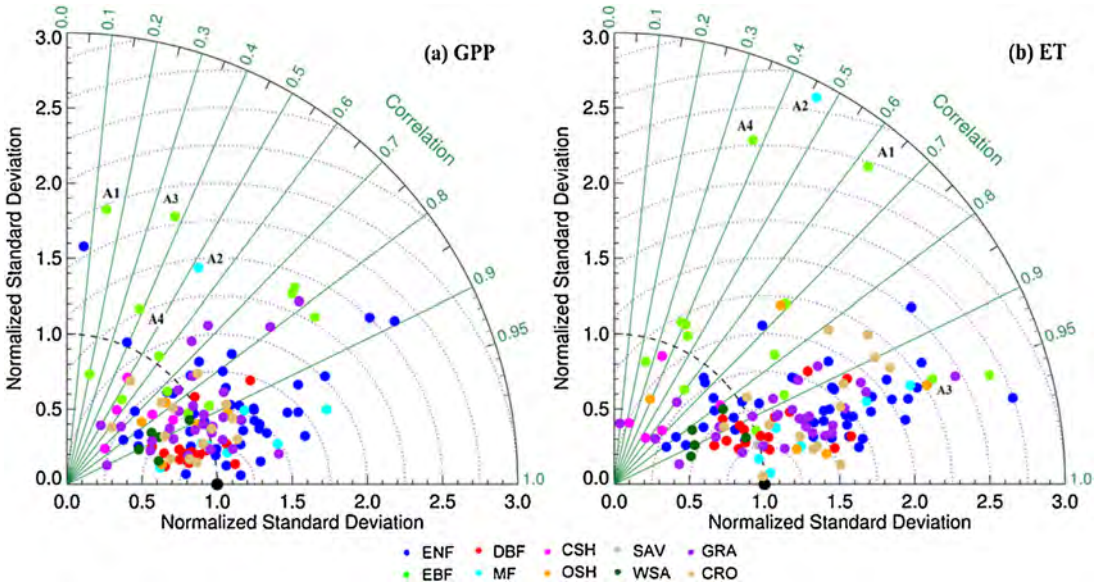

Fig. 9. Taylor diagrams for model performance of GPP (a) and ET (b) estimated by CCW across flux tower sites based on the validation dataset. The cosine of the angle from the X axis is the correlation coefficient between simulated and observed values shown in dark green color. The radial direction is the ratio of simulated to observed standard deviation (i.e., SD, normalized by reference standard deviation). The black point in (a) and (b) is the observed point. The distance between colored and black points is the root mean squared difference (i.e., RMSD, normalized by reference SD) between observed and simulated values at each flux tower site. The purple dashed line is the contour of RMSD with an increment of 0.25. An ideal model would approach the black point with both SD and correlation close to 1. The marked flux tower sites on the plots include BR-Sa1 (A1), JP-Tef (A2), BR-Ji2 (A3), CA-NS4 (A4). Different colors indicate different biomes and their abbreviations are given in Fig. 1. (For interpretation of the references to colour in this figure legend, the reader is referred to the web version of this article.)

underestimated potential LUEs for several biomes, especially for CRO (Madani et al., 2014). In contrast, the updated potential LUE for CRO was generally consistent with the averaged potential LUE used in CCW (Fig. 12).

As a carbon-centric model, CCW calculated ET by using ecosystem WUE and simulated GPP. In this study, we examined three kinds of WUEs and found that UWUE best described the coupling of GPP and ET for most biomes at the monthly scale (Table 3). Physiologically, canopy GPP is only coupled with transpiration (T), but not evaporation (E) from wet leaves and soil surface (Mu et al., 2007, 2011). In this study, we calculated different WUEs directly using monthly ET, but not T, because 1) currently it is difficult to effectively separate T and E from in-situ ET measurements (Wang and Dickinson, 2012), and 2) our aim is to estimate ET, not T only. The involvement of E may influence the effectiveness of the selected WUEs and decouple the relationships between GPP and T. However, given our model was calibrated on ET, the effect of E is also accounted for. The value of WUE would certainly be different if we estimate WUE based on T only, but we will need to further estimate E separately. Whether this will provide an improved estimate

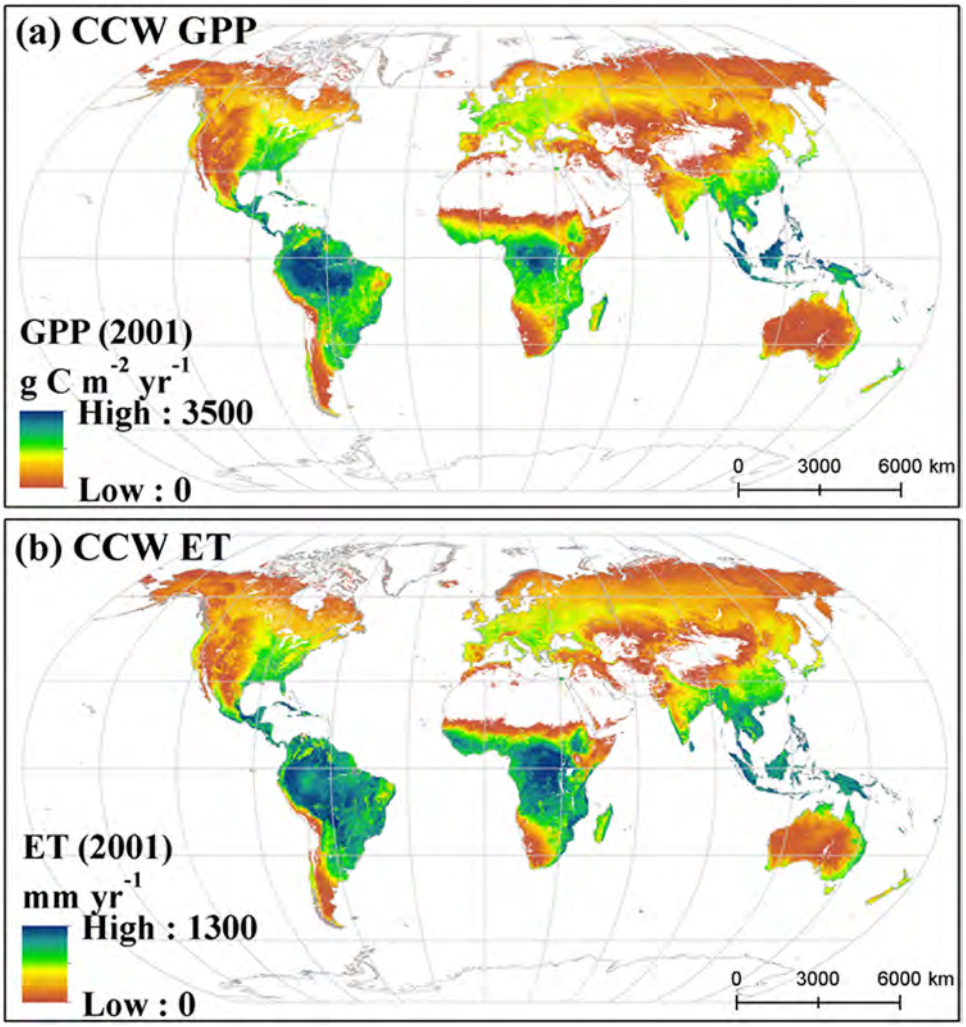

Fig. 10. Spatial patterns of global annual GPP (a) and ET (b) for vegetated surfaces estimated by CCW using MODIS and CRU-NCEP climate data at a spatial resolution of $0.05^\circ \times 0.05^\circ$ for the year 2001. Non-vegetated areas are masked out. (For interpretation of the references to colour in this figure legend, the reader is referred to the web version of this article.)

of ET is worthy of study. However, the fact that our model compared well with the more sophisticated ET algorithm (i.e., MODIS ET) indicates this approach is acceptable. By excluding days with precipitation and a certain interval of subsequent days when the E is low, Zhou et al. (2015) calculated the averaged R^2 of ET versus GPP × $VPD^{0.5}$ (i.e., UWUE), and ET versus GPP × VPD (i.e., IWUE) at the daily scale as 0.72 and 0.66, respectively, which are slightly higher than the monthly values derived in our study (i.e., 0.68 and 0.62). However, the superiority of UWUE over IWUE seems not to significantly change on different temporal scales or whether to exclude evaporation, reflecting the robustness of non-linear effect of VPD on GPP-ET coupling. Both UWUE and IWUE did not do as well as WUE in describing the linkage between GPP and ET for the biomes of MF and WSA (Table 3), probably due to the heterogeneity in these biomes. We compared three WUE-based ET models, and found that ET_{UWUE} showed the best performance to match the tower-measured ET (Fig. 5), suggesting a new effective way to predict ET through a carbon-centric model. In CCW, we did not use precipitation or soil moisture data, but chose VPD to assess the influence of water on GPP and thus ET. This could avoid fully simulating soil water balance on the spatial scale, which is still a big challenge at the moment (Wang and Dickinson, 2012). Further independent validations showed that ET_{UWUE} as well as GPP_{AND} were robust and reliable across most biomes (Figs. 4 and 6) and flux tower sites (Fig. 9). However, large differences between predicted and observed GPP and ET values still existed in a few sites (Fig. 9), reflecting some large variability across sites that were not captured by CCW.

4.2. Model performance at the spatial scale

Accurately estimating global GPP and ET is important to understand and close global carbon and water budgets. Based on CCW, we estimated global GPP for the year 2001 at 134 Pg C yr^{-1} (1 Pg = 10^{15} g), which is close to the value (132 Pg C yr^{-1}) estimated by a process-based model that considered foliage clumping effects (Chen et al., 2012) and the value (136 Pg C yr^{-1}) from the 'optimal' integration of multiple terrestrial biosphere models (Schwalm et al., 2015). However, global GPP by CCW is about 19% higher than MODIS GPP (109.0 Pg C yr^{-1}). Our evaluation showed that the 2001 MODIS GPP was systematically underestimated as much as 17% when compared with FLUXNET tower-derived GPP (Fig. 3c and g). An independent evaluation from Liu et al. (2014) also suggested that MODIS GPP were underestimated for all examined sites from ChinaFLUX. The underestimation of MODIS GPP is probably due to the lack of consideration of diffuse radiation effect on LUE. A recent study from Wang et al. (2015) using flux tower data in China also showed that integration of diffuse radiation effect into MODIS

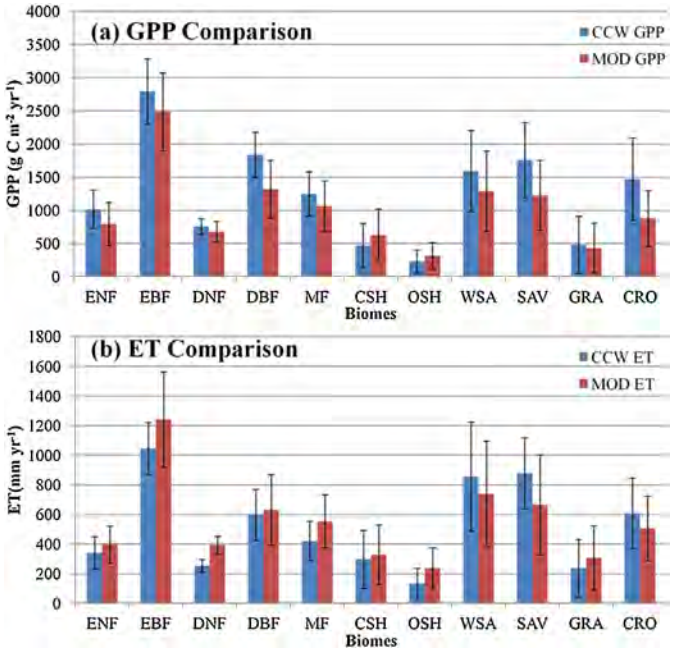

Fig. 11. Comparisons of global averaged GPP (a) and ET (b) from CCW and MODIS for different biomes in 2001. MOD GPP and MOD ET are MODIS products of MOD17 and MOD16, respectively. The black line indicates a standard deviation within each biome. Biome abbreviations are given in Fig. 1. (For interpretation of the references to colour in this figure legend, the reader is referred to the web version of this article.)

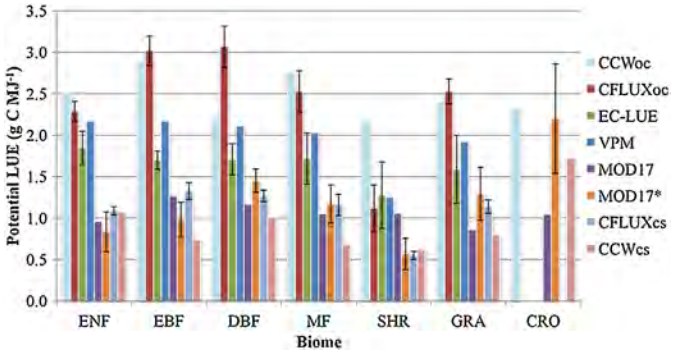

Fig. 12. Comparisons of potential LUEs among LUE models. CCWoc (CFLUXoc) and CCWcs (CFLUXcs) are respectively the potential LUEs under overcast and clear-sky conditions for CCW (CFLUX). The potential LUEs for CFLUX, EC-LUE and VPD are from Yuan et al. (2014). The potential LUEs for MOD17 and MOD17* are from Zhao and Running (2010) and Madani et al. (2014), respectively. The black lines indicate the magnitudes of standard deviations. For CCW, MOD17 and MOD17*, the potential LUE for shrub (SHR) is the averaged value between closed and open shrubs. Other biome abbreviations are given in Fig. 1. (For interpretation of the references to colour in this figure legend, the reader is referred to the web version of this article.)

algorithm could significantly reduce the underestimation of MODIS GPP. Globally, without considering the diffuse radiation effect, GPP tends to be underestimated over humid regions with high diffuse radiation proportion, but overestimated in dry regions with low diffuse proportion. Given the humid regions, especially the tropical and subtropical regions are warmer and wetter, these regions generally have higher GPP than other regions. Although the effect of the underestimation of GPP in humid regions could be offset to some extent by the overestimation of GPP in dry regions, this does not change the overall underestimation of global MODIS GPP (Fig. S2). As the CRO biome is less sensitive to diffuse radiation than other biomes (Fig. 7a and b), the underestimation of MODIS GPP over temperate agricultural regions (e.g., western Europe, eastern U.S. and China; Fig. S2) when compared with CCW GPP might be due to the underestimation of potential LUE for CRO used in MODIS GPP model (Fig. 11; Chen et al., 2011; Madani et al., 2014; Turner et al., 2006a). Based on flux tower data and diagnostic models, Beer et al. (2010) estimated global GPP at 123 ± 8 Pg C yr^{-1}. However, using the oxygen isotopes of atmospheric CO_2 driven by El Niño, Welp et al. (2011) suggested that the current 120 Pg C yr^{-1} is too low to reflect the observed rapid cycling of CO_2, and the best guess of global GPP should be in the range of 150–170 Pg C yr^{-1}. After incorporating the C4 plant distribution in a carbon cycle model, Still et al. (2003) estimated the global GPP to be 150 Pg C yr^{-1}. Cai et al. (2014) evaluated seven LUE models and estimated global GPP in a range of 95–140 Pg C yr^{-1}, while Anav et al. (2015) reviewed ten up-to-date offline and online land surface models and found global GPP estimation varying from 112 to 169 Pg C yr^{-1}. The large differences in global terrestrial GPP derived from different models might be related to uncertainties from model algorithms, observation data, and model input data (Dietze et al., 2011). Although we did not distinguish the distributions of C3 and C4 plants, the difference is inherently built into the model parameters because CCW was calibrated with observed data. Global GPP estimated by CCW suggests the importance of incorporating the diffuse radiation effect into current LUE models.

Global ET estimated by CCW for vegetated areas (75% of land surface based on MODIS land cover product) was 57.0×10^3 km^3 in 2001, very close to MODIS ET (60.5×10^3 km^3). Our site-level evaluation showed that MODIS ET had almost no systematic discrepancy with tower-measured ET (Fig. 5d & h). Both global CCW ET and MODIS ET fell within the model range (i.e., $43.5–63.8 \times 10^3$ km^3 given the assumption that unvegetated areas have the same ET as vegetated areas) estimated by the Global Soil Wetness Project 2 (Dirmeyer et al., 2006). We calculated global total precipitation for vegetated areas in 2001 based on CRU-NCEP data, which was 94.2×10^3 km^3 (or 863 ± 656 mm yr^{-1}). Assuming 60% of global precipitation would return from land to the atmosphere as ET (Oki and Kanae, 2006), the actual ET in 2001 should be 56.5×10^3 km^3, a value very close to global CCW ET. However, the algorithm used to estimate MODIS ET is much more complex, and primarily based on the Penman-Monteith equation at a daily scale (Mu et al., 2011), while CCW ET algorithm is much simpler.

Although there is no direct measurement of ET over large areas, the difference between precipitation (P) and stream flow (Q) (here designated as P–Q) could provide an indirect estimate of ET at the catchment scale over a relatively long period based on the assumption that there is no big change in soil water storage (Mu et al., 2011). We further compared the performances of CCW ET and MODIS ET in 2001 with multi-year (1990–2009) averaged P–Q over 421 U.S. Geological Survey gauged watersheds (Fig. 13). Overall, CCW ET explained 53.5% of spatial variations of P–Q for all watersheds, slightly higher than MODIS ET (52.0%). For both CCW ET and MODIS ET, about 60% of total watersheds showed relative differences between modeled ET and P–Q less than ±20%, which were mainly located in the middle and southeastern regions of the US. CCW ET well captured the variations of P–Q in northeastern US where MODIS ET was significantly overestimated (>30%) probably due to the quality of climate data in this region. However, both CCW ET and MODIS ET were significantly underestimated in the dry western regions and overestimated in wet northwestern regions, respectively. These obvious inconsistencies may be partially due to the variation of a single year modeled ET from the long-term mean ET from P–Q, and they may also reflect the limitations of remote-sensing based methods in ET estimation or the uncertainties in P–Q related to different factors (e.g., surface water measurement errors, ground water withdrawals for artificial usage, extreme climate, etc; Emanuel et al., 2015), which need to be further studied.

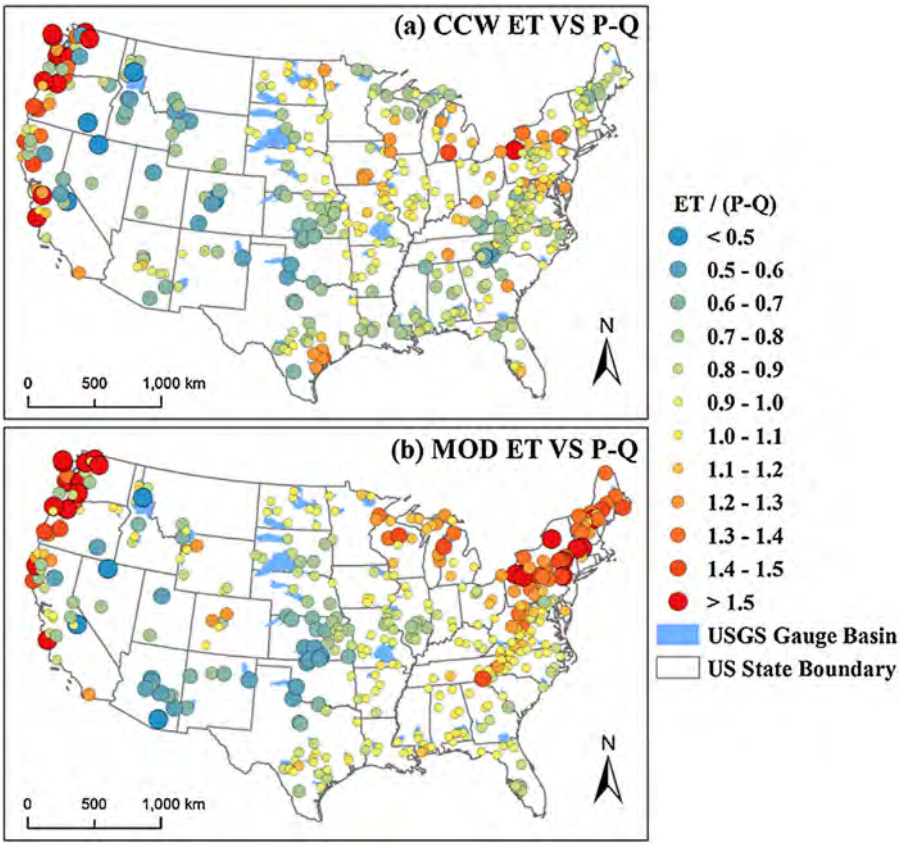

Fig. 13. A comparison of annual ET estimated from CCW (a) and MODIS (b) for the year 2001 with the multi-year averaged (1990–2009) difference between precipitation (P) and measured stream flow (Q) (designated as P–Q) data at 421 U.S. Geological Survey (USGS) gauged reference watersheds. Deviation of the ratio of ET to P–Q from 1.0 indicates model bias. (For interpretation of the references to colour in this figure legend, the reader is referred to the web version of this article.)

4.3. Model advantages and limitations

As a remote-sensing based data-driven model, CCW effectively couples carbon and water in a simple framework. Compared to those complex models that fully consider the physiological (e.g., Farquhar et al., 1980), hydrological (e.g., Monteith 1965) or biogeochemistry (e.g., Parton et al., 1993) processes, CCW is efficient to simulate carbon and water dynamics at different spatial and temporal scales when the remote sensing data is available. Those process-based models, such as LPJ (Sitch et al., 2003), ORCHIDEE (Krinner et al., 2005), SiB2 (Lokupitiya et al., 2009), and CLM4CN (Lawrence et al., 2011), use more complex algorithms in the models, and require detailed spatial input data, many of which are difficult to obtain, or obtainable but with limited accuracy, limiting their potential in real world applications. CCW operates at the monthly scale rather than daily or 8-day scale, which not only balances the tradeoff between data availability and computing efficiency, but also comply with the biological basis behind LUE theory (Song et al., 2013). The basic assumption for LUE model is the linear response of photosynthesis to APAR without other environmental stresses (Monteith, 1972). However, this assumption can hardly be held at short temporal scales (e.g., daily or 8-day), since the photosynthesis-light response curve is highly non-linear in such periods due to the heterogeneity in atmospheric conditions, vegetation leaf structures, and biochemical composition (Ollinger et al., 2008). Based on the modeling results from a closed canopy loblolly pine stand, Song et al. (2013) showed that the cumulative LUE tends to converge at a stable value in about a month, suggesting that the non-linear interactions between photosynthesis rate and APAR at short temporal scale converge to a linear relationship over a longer period as a result of mutual shading of leaves, variation of leaf orientation, and changes in solar zenith angle (Sellers, 1985). Based on the global flux tower data, Zhang et al. (2015) also found that most moisture scalars are generally more effectively modeled in affecting LUE at the monthly scale than at the daily or 8-day scales.

A large number of eco-hydrological factors and processes are related to terrestrial GPP and ET. After calibration of key model parameters based on global flux tower data, CCW explained over 65% of variations of tower-derived GPP (Fig. 3) and ET (Fig. 5). The unexplained variations by CCW may be related to uncertainties of model input data and limitations of the model algorithm. GPP derived from flux tower is not strictly observed data, but rather estimated from measured daytime NEE and estimated daytime respiration. Currently, the extrapolation of night respiration (or night NEE) to daytime respiration still carries large uncertainties (Reichstein et al., 2005; Speckman et al., 2014). Moreover, tower-measured NEE as well as latent heat (or ET) suffer from the problem of surface energy balance closure and tend to be underestimated in most cases (Foken 2008; Wilson et al., 2002). Overall, tower-based GPP and ET are estimated to have 10%–30% errors (Glenn et al., 2008; Schaefer et al., 2012). These errors, which may be randomly distributed over different sites, directly propagate into the parameters used in CCW. Additionally, the tower-based measurement represent the flux integrated over the tower "footprint", the size and shape of which depend on wind speed and direction, surface roughness, canopy height, and atmospheric stability (Schmid, 2002). In this study, we extracted the MODIS NDVI value at $1 \times 1\,km^2$ pixel encompassing each tower site to calculate FPAR. Although the flux tower "footprint" size is generally less than $1 \times 1\,km^2$, there is still a potential mismatch between the derived GPP or ET and calculated FPAR, adding extra uncertainty into CCW. In this study, we calibrated CCW based on the data from over 140

flux tower sites (Table 1). However, these sites are not evenly distributed over space. Some biomes (e.g., SAV, OSH) have very limited sites after data screening, making them less representative for the globe. This situation would be improved as more high-quality flux data become available in the future.

In CCW, we treated the canopy as a "big leaf" and quantified the effect of diffuse radiation on LUE using a linear function of CI (Eq. (4)), which largely simplified the process of canopy radiation transfer over different biomes. However, the effectiveness of CI function under various sky conditions, especially extreme conditions (e.g., completely overcast or clear-sky) needs to be further evaluated based on process-based models (Song et al., 2009). To estimate ET from GPP, we adopted the concept of UWUE, which appeared to be more conservative than other forms of WUE in most biomes (Table S2). However, we assumed UWUE was constant within biome and over time in CCW, which may ignore its potential spatial and seasonal variations caused by factors such as heterogeneity of vegetation structure and seasonal changes of ambient CO_2 (Zhou et al., 2014). Beer et al. (2009) showed that the spatial pattern of IWUE is related to projected foliage cover and soil water content at field capacity. A similar investigation of UWUE could better improve the spatial and temporal estimations of ET by CCW in the future. Other factors including stand age, CO_2 fertilization, nitrogen limitation, and species composition are also omitted in the algorithm of CCW. Despite the limitations mentioned above, the main advantage of CCW is its simplicity with sound biophysical basis, and reasonable accuracy compared to the more complex models. The model framework identified in CCW could be applied on different spatial scales after proper calibrations with more available EC data. Furthermore, the biome-specific parameters derived from this study allows CCW to be further used to investigate the effects of climate change in conjunction with land-use/land-cover change on terrestrial ecosystem functions (Zhang et al., 2014).

5. Conclusions

In this study, we developed a monthly ecosystem model based on global FLUXNET and MODIS data. As a carbon-centric model, CCW estimated GPP based on LUE theory, and calculated ET based on WUE. The model framework was developed by comparing two kinds of GPP models and three kinds of ET models. Overall, CCW could explain 67.3% and 65.7% of tower-measured GPP and ET, respectively. Global GPP and ET estimated by CCW for vegetated areas in 2001 were 134.2 Pg C yr^{-1} and 57.0 × 10^3 km^3, respectively. Global WUE estimated by CCW (2.35 g C kg^{-1} H_2O) was close to the mean tower-based WUE (2.60 g C kg^{-1} H_2O), but higher than the WUE derived from MODIS products (1.80 g C kg^{-1} H_2O). We concluded that the new CCW model provided improved estimates of GPP and ET in a much simpler modeling framework. CCW not only avoids fully simulating soil moisture processes, which currently is still a big challenge, but also provides an independent reference for ET. The biome-specific parameters derived allow CCW to be further linked with land use change models to study the impacts of human activities on ecosystem functions.

Acknowledgements

The EC database used in this study was from FLUXNET, a global network of micrometeorological tower sites gathered from a series of regional networks including: CarboeuropeIP, AmeriFlux, Fluxnet-Canada, LBA, Asiaflux, Chinaflux, USCCC, Ozflux,

Carboafrica, Koflux, NECC, TCOS-Siberia and AfriFlux (http://www.fluxdata.org/). We appreciate the flux tower PIs who made these data freely available and all the other people who were involved in the tower field work. This work was financially supported by the UNC-USDA Forest Service-Joint Venture Agreement (14-JV-11330110-045), National Science Foundation of U.S. (DEB-1313756) and Natural Science Foundation of China (31528004).

Appendix A. Supplementary data

Supplementary data associated with this article can be found, in the online version, at http://dx.doi.org/10.1016/j.agrformet.2016.04.003.

References

Anav, A., Friedlingstein, P., Beer, C., Ciais, P., Harper, A., Jones, C., Murray-Tortarolo, G., Papale, D., Parazoo, N.C., Peylin, P., 2015. Spatiotemporal patterns of terrestrial gross primary production: a review. Rev. Geophys., http://dx.doi.org/10.1002/2015rg000483.

Beer, C., Ciais, P., Reichstein, M., Baldocchi, D., Law, B., Papale, D., Soussana, J.F., Ammann, C., Buchmann, N., Frank, D., 2009. Temporal and among-site variability of inherent water use efficiency at the ecosystem level. Global Biogeochem. Cycles, 23.

Beer, C., Reichstein, M., Tomelleri, E., Ciais, P., Jung, M., Carvalhais, N., Rödenbeck, C., Arain, M.A., Baldocchi, D., Bonan, G.B., 2010. Terrestrial gross carbon dioxide uptake: global distribution and covariation with climate. Science 329, 834–838.

Bosch, J.M., Hewlett, J., 1982. A review of catchment experiments to determine the effect of vegetation changes on water yield and evapotranspiration. J. Hydrol. 55, 3–23.

Cai, W., Yuan, W., Liang, S., Liu, S., Dong, W., Chen, Y., Liu, D., Zhang, H., 2014. Large differences in terrestrial vegetation production derived from satellite-Based light use efficiency models. Remote Sensing 6, 8945–8965.

Castellvi, F., Perez, P., Villar, J., Rosell, J., 1996. Analysis of methods for estimating vapor pressure deficits and relative humidity. Agric. Forest Meteorol. 82, 29–45.

Chatterjee, S., Hadi, A.S., 1986. Influential observations, high leverage points, and outliers in linear regression. Stat. Sci., 379–393.

Chen, T., van der Werf, G.R., Dolman, A., Groenendijk, M., 2011. Evaluation of cropland maximum light use efficiency using eddy flux measurements in North America and Europe. Geophys. Res. Lett. 38.

Chen, J.M., Mo, G., Pisek, J., Liu, J., Deng, F., Ishizawa, M., Chan, D., 2012. Effects of foliage clumping on the estimation of global terrestrial gross primary productivity. Global Biogeochem. Cycles 26, http://dx.doi.org/10.1029/2010gb003996.

Dietze, M.C., Vargas, R., Richardson, A.D., Stoy, P.C., Barr, A.G., Anderson, R.S., Arain, M.A., Baker, I.T., Black, T.A., Chen, J.M., 2011. Characterizing the performance of ecosystem models across time scales: a spectral analysis of the North American Carbon Program site-level synthesis. J. Geophys. Res.: Biogeosci. (2005–2012), 116.

Dirmeyer, P.A., Gao, X., Zhao, M., Guo, Z., Oki, T., Hanasaki, N., 2006. GSWP-2: Multimodel analysis and implications for our perception of the land surface. Bull. Am. Meteorol. Soc. 87, 1381–1397.

Emanuel, R.E., Buckley, J.J., Caldwell, P.V., McNulty, S.G., Sun, G., 2015. Influence of basin characteristics on the effectiveness and downstream reach of interbasin water transfers: displacing a problem. Environ. Res. Lett. 10 (12), 124005–124013.

Fang, Y., Sun, G., Caldwell, P., McNulty, S., Noormets, A., Domec, J., King, J., Zhang, Z., Zhang, X., Lin, G., Xiao, J., Chen, J., 2015. Monthly land cover-specific evapotranspiration models derived from global eddy flux measurements and remote sensing data. Ecohydrology, http://dx.doi.org/10.1002/eco.1629.

Farquhar, G., von Caemmerer, S.v., Berry, J., 1980. A biochemical model of photosynthetic CO_2 assimilation in leaves of C3 species. Planta 149, 78–90.

Foken, T., 2008. The energy balance closure problem: an overview. Ecol. Appl. 18, 1351–1367.

Glenn, E.P., Morino, K., Didan, K., Jordan, F.C., Carroll, K., Nagler, P.L., Hultine, K., Sheader, L., Waugh, J., 2008. Scaling sap flux measurements of grazed and ungrazed shrub communities with fine and coarse-resolution remote sensing. Ecohydrology 1, 316–329.

Gu, L., Baldocchi, D., Verma, S.B., Black, T., Vesala, T., Falge, E.M., Dowty, P.R., 2002. Advantages of diffuse radiation for terrestrial ecosystem productivity. J. Geophys. Res.: Atmos. (1984–2012) 107, 2–11.

Hashimoto, H., Wang, W., Milesi, C., Xiong, J., Ganguly, S., Zhu, Z., Nemani, R.R., 2013. Structural uncertainty in model-simulated trends of global gross primary production. Remote Sens. 5, 1258–1273.

Hu, Z., Yu, G., Zhou, Y., Sun, X., Li, Y., Shi, P., Wang, Y., Song, X., Zheng, Z., Zhang, L., 2009. Partitioning of evapotranspiration and its controls in four grassland ecosystems: application of a two-source model. Agric. Forest Meteorol. 149, 1410–1420.

Hu, Z., Li, S., Yu, G., Sun, X., Zhang, L., Han, S., Li, Y., 2013. Modeling evapotranspiration by combing a two-source model, a leaf stomatal model: and a light-use efficiency model. J. Hydrol. 501, 186–192.

Jönsson, P., Eklundh, L., 2004. TIMESAT—a program for analyzing time-series of satellite sensor data. Comput. Geosci. 30, 833–845.

Janssen, P., Heuberger, P., 1995. Calibration of process-oriented models. Ecol. Modell. 83, 55–66.

Jarvis, P., 1976. The interpretation of the variations in leaf water potential and stomatal conductance found in canopies in the field. Philos. Trans. R. Soc. Lond. B: Biol. Sci. 273, 593–610.
Kanniah, K.D., Beringer, J., North, P., Hutley, L., 2012. Control of atmospheric particles on diffuse radiation and terrestrial plant productivity A review. Prog. Phys. Geogr. 36, 209–237.
King, D.A., Turner, D.P., Ritts, W.D., 2011. Parameterization of a diagnostic carbon cycle model for continental scale application. Remote Sens. Environ. 115, 1653–1664.
Koster, R.D., Dirmeyer, P.A., Guo, Z., Bonan, G., Chan, E., Cox, P., Gordon, C., Kanae, S., Kowalczyk, E., Lawrence, D., 2004. Regions of strong coupling between soil moisture and precipitation. Science 305, 1138–1140.
Krause, P., Boyle, D., Bäse, F., 2005. Comparison of different efficiency criteria for hydrological model assessment. Adv. Geosci. 5, 89–97.
Krinner, G., Viovy, N., de Noblet-Ducoudré, N., Ogée, J., Polcher, J., Friedlingstein, P., Ciais, P., Sitch, S., Prentice, I.C., 2005. A dynamic global vegetation model for studies of the coupled atmosphere-biosphere system. Global Biogeochem. Cycles 19.
Landsberg, J., Waring, R., 1997. A generalised model of forest productivity using simplified concepts of radiation-use efficiency: carbon balance and partitioning. For. Ecol. Manage. 95, 209–228.
Law, B., Falge, E., Gu L. v. Baldocchi, D., Bakwin, P., Berbigier, P., Davis, K., Dolman, A., Falk, M., Fuentes, J., 2002. Environmental controls over carbon dioxide and water vapor exchange of terrestrial vegetation. Agric. Forest Meteorol. 113, 97–120.
Lawrence, D.M., Oleson, K.W., Flanner, M.G., Thornton, P.E., Swenson, S.C., Lawrence, P.J., Zeng, X., Yang, Z.L., Levis, S., Sakaguchi, K., 2011. Parameterization improvements and functional and structural advances in version 4 of the Community Land Model. J. Adv. Model. Earth Syst. 3.
Le Quéré, C., Raupach, M.R., Canadell, J.G., Marland, G., Bopp, L., Ciais, P., Conway, T.J., Doney, S.C., Feely, R.A., Foster, P., 2009. Trends in the sources and sinks of carbon dioxide. Nat. Geosci. 2, 831–836.
Liu, Z., Shao, Q., Liu, J., 2014. The performances of MODIS-GPP and-ET products in China and their sensitivity to input data (FPAR/LAI). Remote Sens. 7, 135–152.
Lokupitiya, E., Denning, S., Paustian, K., Baker, I., Schaefer, K., Verma, S., Meyers, T., Bernacchi, C., Suyker, A., Fischer, M., 2009. Incorporation of crop phenology in Simple Biosphere Model (SiBcrop) to improve land-atmosphere carbon exchanges from croplands. Biogeosciences 6, 969–986.
Madani, N., Kimball, J.S., Affleck, D.L., Kattge, J., Graham, J., Bodegom, P.M., Reich, P.B., Running, S.W., 2014. Improving ecosystem productivity modeling through spatially explicit estimation of optimal light use efficiency. J. Geophys. Res.: Biogeosci. 119, 1755–1769.
McGuire, A., Sitch, S., Clein, J., Dargaville, R., Esser, G., Foley, J., Heimann, M., Joos, F., Kaplan, J., Kicklighter, D., 2001. Carbon balance of the terrestrial biosphere in the twentieth century: analyses of CO_2: climate and land use effects with four process-based ecosystem models. Global Biogeochem. Cycles 15, 183–206.
Medlyn, B.E., 1998. Physiological basis of the light use efficiency model. Tree Physiol. 18, 167–176.
Mercado, L.M., Bellouin, N., Sitch, S., Boucher, O., Huntingford, C., Wild, M., Cox, P.M., 2009. Impact of changes in diffuse radiation on the global land carbon sink. Nature 458, 1014–1017.
Monteith, J., 1965. Evaporation and environment. Symp. Soc. Exp. Biol. 4.
Monteith, J., 1972. Solar radiation and productivity in tropical ecosystems. J. Appl. Ecol. 9, 747–766.
Mu, Q., Heinsch, F.A., Zhao, M., Running, S.W., 2007. Development of a global evapotranspiration algorithm based on MODIS and global meteorology data. Remote Sens. Environ. 111, 519–536.
Mu, Q., Zhao, M., Running, S.W., 2011. Improvements to a MODIS global terrestrial evapotranspiration algorithm. Remote Sens. Environ. 115, 1781–1800.
Myneni, R., Williams, D., 1994. On the relationship between FAPAR and NDVI. Remote Sens. Environ. 49, 200–211.
Nole, A., Law, B., Magnani, F., Matteucci, G., Ferrara, A., Ripullone, F., Borghetti, M., 2009. Application of the 3-PGS model to assess carbon accumulation in forest ecosystems at a regional level. Can. J. For. Res. 39, 1647–1661.
Oki, T., Kanae, S., 2006. Global hydrological cycles and world water resources. Science 313, 1068–1072.
Ollinger, S., Richardson, A., Martin, M., Hollinger, D., Frolking, S., Reich, P., Plourde, L., Katul, G., Munger, J., Oren, R., 2008. Canopy nitrogen, carbon assimilation, and albedo in temperate and boreal forests: functional relations and potential climate feedbacks. Proc. Natl. Acad. Sci. 105, 19336–19341.
Parton, W., Scurlock, J., Ojima, D., Gilmanov, T., Scholes, R., Schimel, D.S., Kirchner, T., Menaut, J.C., Seastedt, T., Garcia Moya, E., 1993. Observations and modeling of biomass and soil organic matter dynamics for the grassland biome worldwide. Global Biogeochem. Cycles 7, 785–809.
Ponton, S., Flanagan, L.B., Alstad, K.P., Johnson, B.G., Morgenstern, K., Kljun, N., BLACK, T.A., Barr, A.G., 2006. Comparison of ecosystem water-use efficiency among Douglas-fir forest, aspen forest and grassland using eddy covariance and carbon isotope techniques. Global Change Biol. 12, 294–310.
Potter, C.S., Randerson, J.T., Field, C.B., Matson, P.A., Vitousek, P.M., Mooney, H.A., Klooster, S.A., 1993. Terrestrial ecosystem production: a process model based on global satellite and surface data. Global Biogeochem. Cycles 7, 811–841.
Raes, D., Steduto, P., Hsiao, T.C., Fereres, E., 2009. AquaCrop the FAO crop model to simulate yield response to water: II: Main algorithms and software description. Agron. J. 101, 438–447.
Raich, J., Rastetter, E., Melillo, J., Kicklighter, D., Steudler, P., Peterson, B., Grace, A., Moore Iii, B., Vorosmarty, C., 1991. Potential net primary productivity in South America: application of a global model. Ecol. Appl. 1, 399–429.
Reichstein, M., Falge, E., Baldocchi, D., Papale, D., Aubinet, M., Berbigier, P., Bernhofer, C., Buchmann, N., Gilmanov, T., Granier, A., 2005. On the separation of net ecosystem exchange into assimilation and ecosystem respiration: review and improved algorithm. Global Change Biol. 11, 1424–1439.
Running, S.W., Thornton, P.E., Nemani, R., Glassy, J.M., 2000. Global terrestrial gross and net primary productivity from the Earth Observing System. In: Methods in Ecosystem Science. Springer, pp. 44–57.
Running, S.W., Nemani, R.R., Heinsch, F.A., Zhao, M., Reeves, M., Hashimoto, H., 2004. A continuous satellite-derived measure of global terrestrial primary production. Bioscience 54, 547–560.
Running, S.W., 2012. A measurable planetary boundary for the biosphere. Science 337, 1458–1459.
Schaefer, K., Schwalm, C.R., Williams, C., Arain, M.A., Barr, A., Chen, J.M., Davis, K.J., Dimitrov, D., Hilton, T.W., Hollinger, D.Y., 2012. A model-data comparison of gross primary productivity: results from the North American Carbon Program site synthesis. J. Geophys. Res.: Biogeosci. (2005–2012), 117.
Schmid, H.P., 2002. Footprint modeling for vegetation atmosphere exchange studies: a review and perspective. Agric. Forest Meteorol. 113, 159–183.
Schwalm, C.R., Huntinzger, D.N., Fisher, J.B., Michalak, A.M., Bowman, K., Cias, P., Cook, R., El-Masri, B., Hayes, D., Huang, M., 2015. Toward optimal integration of terrestrial biosphere models. Geophys. Res. Lett., http://dx.doi.org/10.1002/2015GL064002.
Sellers, P.J., 1985. Canopy reflectance, photosynthesis and transpiration. Int. J. Remote Sensens. 6 (8), 1335–1372.
Seneviratne, S.I., Lüthi, D., Litschi, M., Schär, C., 2006. Land–atmosphere coupling and climate change in Europe. Nature 443, 205–209.
Sims, D.A., Rahman, A.F., Cordova, V.D., Baldocchi, D.D., Flanagan, L.B., Goldstein, A.H., Hollinger, D.Y., Misson, L., Monson, R.K., Schmid, H.P., 2005. Midday values of gross CO_2 flux and light use efficiency during satellite overpasses can be used to directly estimate eight-day mean flux. Agric. Forest Meteorol. 131, 1–12.
Sitch, S., Smith, B., Prentice, I.C., Arneth, A., Bondeau, A., Cramer, W., Kaplan, J., Levis, S., Lucht, W., Sykes, M.T., 2003. Evaluation of ecosystem dynamics, plant geography and terrestrial carbon cycling in the LP: J dynamic global vegetation model. Global Change Biol. 9, 161–185.
Song, C., Katul, G., Oren, R., Band, L.E., Tague, C.L., Stoy, P.C., McCarthy, H.R., 2009. Energy, water, and carbon fluxes in a loblolly pine stand: results from uniform and gappy canopy models with comparisons to eddy flux data. J. Geophys. Res.: Biogeosci. 114, 2005–2012.
Song, C., Dannenberg, M.P., Hwang, T., 2013. Optical remote sensing of terrestrial ecosystem primary productivity. Prog. Phys. Geogr. 37, 834–854.
Speckman, H.N., Frank, J.M., Bradford, J.B., Miles, B.L., Massman, W.J., Parton, W.J., Ryan, M.G., 2014. Forest ecosystem respiration estimated from eddy covariance and chamber measurements under high turbulence and substantial tree mortality from bark beetles. Global Change Biol.
Still, C.J., Berry, J.A., Collatz, G.J., DeFries, R.S., 2003. Global distribution of C3 and C4 vegetation: carbon cycle implications. Global Biogeochem. Cycles 17 (6-1-6-14).
Sun, G., Alstad, K., Chen, J., Chen, S., Ford, C.R., Lin, G., Liu, C., Lu, N., McNulty, S.G., Miao, H., 2011a. A general predictive model for estimating monthly ecosystem evapotranspiration. Ecohydrology 4, 245–255.
Sun, G., Caldwell, P., Noormets, A., McNulty, S.G., Cohen, E., Moore Myers, J., Domec, J.C., Treasure, E., Mu, Q., Xiao, J., 2011b. Upscaling key ecosystem functions across the conterminous United States by a water-centric ecosystem model. J. Geophys. Res.: Biogeosci. (2005–2012) 116.
Taylor, K.E., 2001. Summarizing multiple aspects of model performance in a single diagram. J. Geophys. Res.: Atmos. (1984–2012) 106, 7183–7192.
Tian, H., Chen, G., Liu, M., Zhang, C., Sun, G., Lu, C., Xu, X., Ren, W., Pan, S., Chappelka, A., 2010. Model estimates of net primary productivity, evapotranspiration: and water use efficiency in the terrestrial ecosystems of the southern United States during 1895–2007. For. Ecol. Manage. 259, 1311–1327.
Turner, D., Ritts, W., Cohen, W., Gower, S., Running, S., Zhao, M., Costa, M., Kirschbaum, A., Ham, J., Saleska, S., 2006a. Evaluation of MODIS NPP and GPP products across multiple biomes. Remote Sens. Environ. 102, 282–292.
Turner, D., Ritts, W., Styles, J., Yang, Z., Cohen, W., Law, B., Thornton, P., 2006b. A diagnostic carbon flux model to monitor the effects of disturbance and interannual variation in climate on regional NEP. Tellus B 58, 476–490.
Wang, K., Dickinson, R.E., 2012. A review of global terrestrial evapotranspiration: observation, modeling, climatology, and climatic variability. Rev. Geophys. 50.
Wang, L., Jacques, S.L., Zheng, L., 1995. MCML—Monte Carlo modeling of light transport in multi-layered tissues. Comput. Methods Progr. Biomed. 47, 131–146.
Wang, W., Ciais, P., Nemani, R.R., Canadell, J.G., Piao, S., Sitch, S., White, M.A., Hashimoto, H., Milesi, C., Myneni, R.B., 2013. Variations in atmospheric CO2 growth rates coupled with tropical temperature. Proc. Natl. Acad. Sci. 110, 13061–13066.
Wang, S., Huang, K., Yan, H., Yan, H., Zhou, L., Wang, H., Zhang, J., Yan, J., Zhao, L., Wang, Y., 2015. Improving the light use efficiency model for simulating terrestrial vegetation gross primary production by the inclusion of diffuse radiation across ecosystems in China. Ecol. Complexity 23, 1–13.
Waring, R.H., Running, S.W., 2010. Forest Ecosystems: Analysis at Multiple Scales. Elsevier.

Welp, L.R., Keeling, R.F., Meijer, H.A., Bollenbacher, A.F., Piper, S.C., Yoshimura, K., Francey, R.J., Allison, C.E., Wahlen, M., 2011. Interannual variability in the oxygen isotopes of atmospheric CO_2 driven by El Niño. Nature 477, 579–582.
Weng, E., Luo, Y., 2008. Soil hydrological properties regulate grassland ecosystem responses to multifactor global change: a modeling analysis. J. Geophys. Res.: Biogeosci. 113, 2005–2012.
Wilson, K.B., Hanson, P.J., Mulholland, P.J., Baldocchi, D.D., Wullschleger, S.D., 2001. A comparison of methods for determining forest evapotranspiration and its components: sap-flow, soil water budget, eddy covariance and catchment water balance. Agric. Forest Meteorol. 106, 153–168.
Wilson, K., Goldstein, A., Falge, E., Aubinet, M., Baldocchi, D., Berbigier, P., Bernhofer, C., Ceulemans, R., Dolman, H., Field, C., 2002. Energy balance closure at FLUXNET sites. Agric. Forest Meteorol. 113, 223–243.
Xiao, X., Zhang, Q., Braswell, B., Urbanski, S., Boles, S., Wofsy, S., Moore, B., Ojima, D., 2004. Modeling gross primary production of temperate deciduous broadleaf forest using satellite images and climate data. Remote Sens. Environ. 91, 256–270.
Yuan, W., Liu, S., Zhou, G., Zhou, G., Tieszen, L.L., Baldocchi, D., Bernhofer, C., Gholz, H., Goldstein, A.H., Goulden, M.L., 2007. Deriving a light use efficiency model from eddy covariance flux data for predicting daily gross primary production across biomes. Agric. Forest Meteorol. 143, 189–207.
Yuan, W., Liu, S., Yu, G., Bonnefond, J.-M., Chen, J., Davis, K., Desai, A.R., Goldstein, A.H., Gianelle, D., Rossi, F., 2010. Global estimates of evapotranspiration and gross primary production based on MODIS and global meteorology data. Remote Sens. Environ. 114, 1416–1431.
Yuan, W., Cai, W., Xia, J., Chen, J., Liu, S., Dong, W., Merbold, L., Law, B., Arain, A., Beringer, J., 2014. Global comparison of light use efficiency models for simulating terrestrial vegetation gross primary production based on the LaThuile database. Agric. Forest Meteorol. 192, 108–120.
Zhang, Y., Song, C., Zhang, K., Cheng, X., Band, L.E., Zhang, Q., 2014. Effects of land-use/land-cover and climate changes on terrestrial net primary productivity in the Yangtze River Basin, China from 2001 to 2010. J. Geophys. Res.: Biogeosci. 119, http://dx.doi.org/10.1002/2014jg002616.
Zhang, Y., Song, C., Sun, G., Band, L.E., Noormets, A., Zhang, Q., 2015. Understanding moisture stress on light-use efficiency across terrestrial ecosystems based on global flux and remote sensing data. J. Geophys. Res.: Biogeosci., http://dx.doi.org/10.1002/2015JG003023.
Zhao, M., Running, S.W., 2010. Drought-induced reduction in global terrestrial net primary production from 2000 through 2009. Science 329, 940–943.
Zhou, S., Yu, B., Huang, Y., Wang, G., 2014. The effect of vapor pressure deficit on water use efficiency at the subdaily time scale. Geophys. Res. Lett. 41, 5005–5013.
Zhou, S., Yu, B., Huang, Y., Wang, G., 2015. Daily underlying water use efficiency for AmeriFlux sites. J. Geophys. Res.: Biogeosci., http://dx.doi.org/10.1002/2015jg002947.